Peer-reviewed version available at *Environmental Science and Technology* **2019**; doi:10.1021/acs.est.9b03105

Raman Tweezers as a Tool for Small Microplastics and Nanoplastics Identification in Sea Water.

Raymond Gillibert,[1] Gireeshkumar Balakrishnan,[2] Quentin Deshoules,[3] Morgan Tardivel,[3] Alessandro Magazzù,[4] Maria Grazia Donato,[1] Onofrio M. Maragò,[1] Marc Lamy de La Chapelle,[2] Florent Colas,[3] Fabienne Lagarde,[2] Pietro G. Gucciardi[1]

[1] CNR – IPCF, Istituto per i Processi Chimico-Fisici, Viale F. Stagno D'Alcontres 27, I- 98158 Messina, Italy

[2] Institut des Molécules et Matériaux du Mans, UMR 6283 CNRS, Université du Maine, Le Mans, France

[3] Ifremer LDCM, Centre Bretagne, CS 10070, 29280 Plouzané, France

[4] Department of Physics, University of Gothenburg, 41296 Gothenburg, Sweden

Keywords: Microplastics, Nanoplastics, Optical Tweezers, Raman Spectroscopy.

ABSTRACT Our understanding of the fate and distribution of micro- and nano- plastics in the marine environment and their impact on the biota compartment is limited by the intrinsic difficulties of conventional analytical techniques (light scattering, FT-IR, Raman, optical and electron microscopies) in the detection, quantification and chemical identification of small particles in liquid samples. Here we propose the use of optical tweezers, a technique awarded in 2018 with the Nobel prize, as an analytical tool for the study of micro- and nano- plastics in sea water. In particular, we exploit the combination of optical tweezers with Raman spectroscopy (Raman Tweezers, RTs) to optically trap plastic particles with sizes from tens of μm down to 90 nm and unambiguously reveal their chemical composition. RTs applications are shown on particles made of the most common plastic pollutants, including polyethylene, polypropylene, nylon and polystyrene, that are artificially fragmented and aged directly in seawater. RTs allow us to assess the size and shapes of microparticles (beads, fragments, fibers) and can be applied to investigate particles covered with organic layers. Furthermore, operating at the single particle level, RTs enable unambiguous distinction of plastic particles from marine microorganisms and seawater minerals, overcoming the capacities of standard Raman spectroscopy in liquid, limited to average measurements. Coupled to suitable extraction and concentration protocols, RTs could have a strong impact in the study of the fate of micro and nanoplastics in marine environment, as well as in the understanding of the fragmentation processes on a multi-scale level.

INTRODUCTION

As much as 75% of all the litter in the oceans is made of plastic.[1,2] Most common examples are: Polyethylene (PE), Polypropylene (PP), Nylon (PA), Polystyrene (PS), Polyethylene terephthalate (PET), Polymethyl methacrylate (PMMA), and Polyvinyl Chloride (PVC). Fragmentation of plastic litter into debris of smaller size due to photophysical, mechanical and biological degradation[3] is a source marine pollution by microplastics[4],[5] (Figure 1). Products of industrial spillage,[6] particles used in cosmetics,[7],[8],[9] in 3D printing[10] and in lubricants[11] represent a further source of small plastic particulate that typically ends its life in the seas. More recently, it has been shown in laboratory that microplastics under continuous light (UV) illumination fragment into nanoscale debris [12],[13],[14] called nanoplastics,[15],[16] that represent a new, yet unexplored form of marine pollution. Preliminary evidence of nanoplastic colloids in the waters of the North Atlantic subtropical gyre has just been reported in 2017. [17] Microplastics and nanoplastics are of great concern as they represent a threat for the biota compartments. They are ingested by lower trophic level organisms with effects ranging from lethal to sub-lethal.[18], [19], [20],[21] Their transfer through the trophic chain[22],[23] is a potential source of contamination at all the trophic levels.

As proposed in the European Water Framework (EWF) directive,[24] plastic particles < 5 mm are named microplastics, with a distinction between large microplastics (1 – 5mm) and small microplastics (< 1mm). [25,26] The lower limit in this definition is, however, undefined.[5] Some authors set it to 20 – 25 µm, corresponding to the minimum mesh size of the trawl nets used for sampling. Others set it to the more natural value of 1µm.[27],[28] Sub-micrometric plastics are generally named nanoplastics, although no precise definition still exists. In fact, some authors call nanoplastics objects from 1 µm to 1 nm,[15,16,17,] while f or others it is required that at least one dimension is < 100nm.[29],[30] Here (Figure 1) we use the EWF definition for the term microplastics

and use the term nanoplastics for particles smaller than 1 µm in at least two dimensions, no matter whether they are produced intentionally (primary nanoplastics, e.g. nanobeads for biological applications,[31] calibration standards[32],[33] or catalysts supports[34]) or unintentionally (secondary nanoplastics, e.g. arising from the degradation or the manufacturing larger plastics).[15] Additionally, we call large nanoplastics those between 1 µm and 100 nm and small nanoplastics the ones smaller than 100 nm.

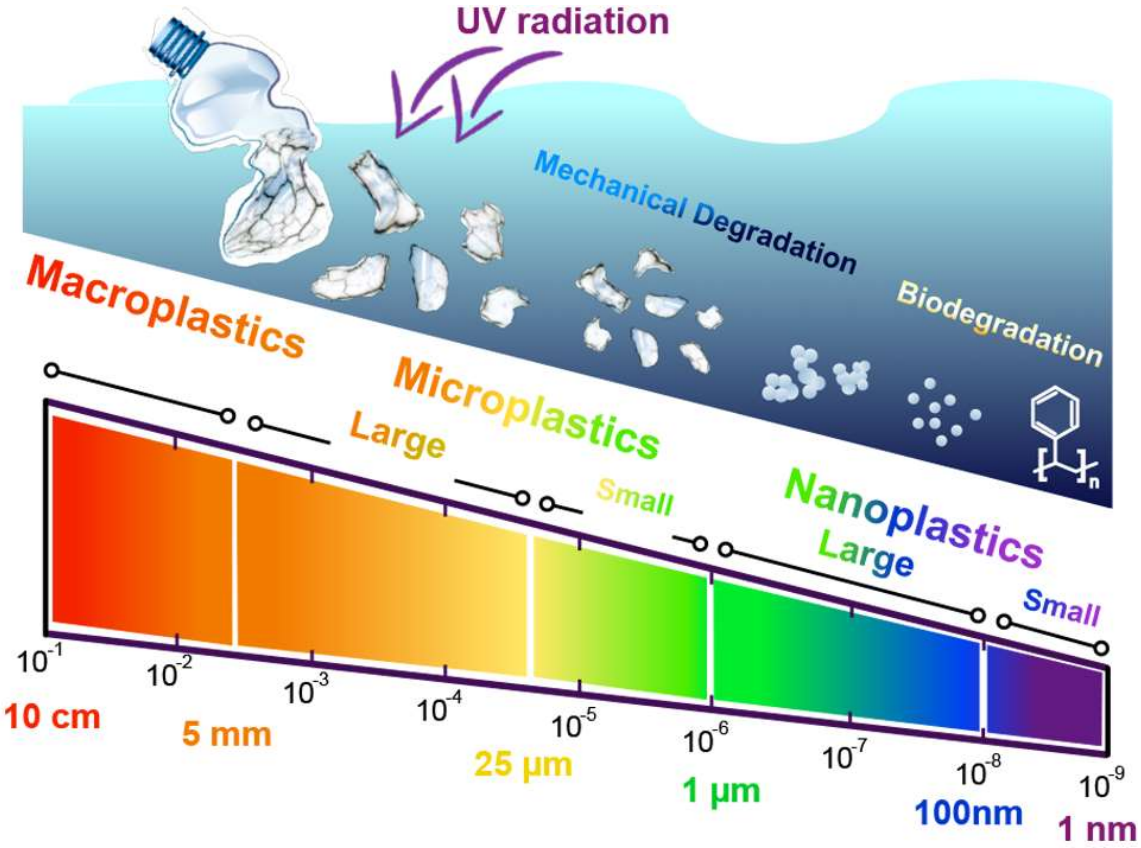

Figure 1: Degradation flow and size-based definition of plastics.

The pathway and ultimate fate of small plastic fragments is still unknown. Nowadays circa $5 \cdot 10^{12}$ small plastic fragments, [35],[36] corresponding to a mass ~ 250 thousand tons, are estimated to float

at the sea surface, following the marine currents. Their presence has been detected in deep-sea waters and sediments.[37],[38] According to a survey made in 2014,[25] however, the quantity of plastics detected in the oceans is orders of magnitude smaller than expected. This is maybe due to the fact that experimental reports are mostly limited to particles of 20 µm in size.[39,40] The undetected micrometric (sub-20 µm) and nanometric fraction could be, therefore, orders of magnitude larger than the investigated sub-mm portion.[25, 12]

The field of small microplastics (< 20 µm) and nanoplastics (< 1µm) is currently perceived as the last unexplored frontier in marine research. Very few studies on 1 – 20 µm microplastics have been carried out in bottled water, [41] sea water,[42] and on their ingestion by zooplankton.[43] The existence of nanoplastics (< 1 µm) in seawater has just been preliminary reported. [17] While for large microplastics protocols for sampling and analysis are well assessed (see Table 1),[44],[45] the lack of standardized procedures for collection and concentration of particles < 20 µm, together with the absence of accepted analytical tools to identify their chemical nature, has been recognized as one of the main challenges to be afforded to solve the missing fraction *conundrum*.[16,46] The techniques used in the few reports published so far on the detection of small microplastics and nanoplastics include (Table 1) Transmission/Scanning Electron Microscopy (TEM/SEM), fluorescence microscopy, Nanoparticles Tracking Analysis (NTA) and Dynamic Light Scattering (DLS). Such means have permitted to demonstrate the occurrence of the particles and give a first size estimate, but none of them is capable to provide chemical information and the definitive proof that the observed particles are really plastics is still lacking. It is a shared opinion, in fact, that methods to characterize the chemical nature of nanoplastics, especially in water environment, are still to be invented.[16,15,12,46,47, 48]

Among the "classical" analytical techniques Raman spectroscopy, indeed, has the potential to probe nanomaterials.[49] Although the spatial resolution is limited by diffraction to ~ 250 nm (in the visible range) the sensitivity is at the single nanostructure level (carbon nanotubes with few nm diameters can be easily analyzed)[50] and plastic particles with sizes of few tens of nanometers can be detected.[51] Nanospectroscopy tools, such as Atomic Force Microscopy – Infrared (AFM-IR),[52] Near-Field Raman Microscopy and Tip-Enhanced Raman Spectroscopy (TERS),[53] or Nano-FTIR[54] offer, in addition, a platform to obtain nanoscale spatial resolutions. Proof-of-concept of the chemical identification possibilities on polymer structures have already been shown.[55],[56],[57] Nanospectroscopy tools (Table 1) are, however, expensive, require bulky setups and vibration-isolated laboratories. None of these setups is capable to analyze particles in liquid dispersions, requiring drying of the samples on flat surfaces.

Table 1: Methods to assess morphology, quantity and chemical nature of micro- and nano- plastics.

Technique	Min particle size	Max particle size	Information / Advantages	Limitations	Use in water	Ref.
Visual inspection, stiffness test	500 µm	cm	Size, shape, color, consistence, materials identification.	Limited accuracy, not suitable for micron scale objects	YES	44
FTIR, µFTIR	10 – 100 µm	cm	Materials identification. Particle size imaging. Portable. Non-invasive	Slow acquisitions, cannot work in water.	NO	39,46,[58],[59]
Raman, µRaman	Tens of nm	cm	Materials identification. Particle size imaging. Portable. Non-invasive	Time consuming, not suited for fluorescent samples.	YES	41,[59],[60],[61]
Raman Tweezers	40nm	50µm	Materials identification. Single particle analysis in water. Particle size imaging.	Not suited for fluorescent samples	YES	

Nanoparticles tracking analysis	30nm	1 µm	Particle size distribution. Concentration estimation. Portable. Non-invasive	No chemical identification.	YES	14
Dynamic Light Scattering	1nm	5 µm	Direct access to size distribution, very good sensitivity. Non-invasive	No chemical identification. No imaging capabilities	YES	12,17
Pyrolysis Gas Chromatography–mass spectroscopy.	-	cm	Chemical identification. Identification in real environmental samples	No particle sizing. Cannot identify mixtures of plastics. Destructive	NO	17,[62],[63,64]
Optical / Fluorescence Microscopy	250nm	mm	Possibility of chemical identification. Particle size imaging.	Labelling needed for particles identification. Chemical identification by colorimetry not always reliable	YES	40,43,[65]
Electron Microscopy / X-Rays (SEM/TEM/EDX)	1nm	mm	Accurate elemental analysis (EDX) and imaging (SEM). Sub-nm resolution (TEM)	Heavy and expensive. Sensitive to vibrations.	NO	15, 41, 63
Near-Field Raman Spectroscopy (SNOM,TERS)	Atomic scale	1µm	Particle size imaging. Chemical identification.	Heavy and expensive.	NO	53,56
Atomic Force Microscopy - IR (AFM-IR)	10nm	100 µm	Imaging. Chemical identification.	Expensive equipment.	NO	52,55
Nano FT-IR	20nm	100µm	Particle size imaging. Chemical identification.	Heavy and expensive.	NO	54,57

Optical tweezers (OT) [66,67] are a tool capable to trap and manipulate micro and nanoparticles dispersed in liquid, [68] by exploiting the tiny forces that light exerts on matter.[69] When coupled to Raman spectrometers, OT enable chemical analysis of the trapped particles. Since the first demonstration of "Raman micro-sampling in an optical trap", [70] the so-called Raman Tweezers (RT)[71] have found applications[72] in several fields including cells sorting,[73],[74] virology,[75] nanomaterials analysis,[76,77,78] Surface Enhanced Raman detection of molecules[79],[80] and biomolecules.[81],[82] First demonstrations of the potentialities of OT/RT in the field of nanoplastics

(although the name was far from being invented) were shown by Ashkin et al. in 1986,[69] with the stable trapping of 25nm PS spheres, and by Ajito *et al.* in 2002, [83] who showed Raman spectra of 40nm diameter PS spheres optically trapped in water. Since then, no other study has been published, to our best knowledge, on the detection by RT of nanoscale plastic particles.

The aim of this article is to show that RTs can be applied to trap and chemically identify a broad range of small micro- and nanoplastics in seawater, and to unambiguously discriminate plastics from other substances commonly found in seawater samples, such as sediments. Results are shown on commercial and artificially fragmented/aged micro- and nanoplastics (90nm – 10 µm diameter) made of PP, PS, PE, Nylon, PVC. Unambiguous size and shape information is additionally retrieved on particles larger than 500 nm.

THEORETICAL BASIS

Optical Forces are due to the momentum exchange between the photons and particles during the light-matter interaction.[66] These forces can be opportunely generated with tightly focused laser beams to confine a particle in an optical potential well, giving rise to the so-called optical trapping. Besides adopting the full electromagnetic theory (complex and computationally intensive), different approximated models can be used to calculate optical forces.[72] The size parameter $x = k_m a$ defines the range of validity of each approximation, where $k_m = 2\pi n_m/\lambda$, is the light wavenumber in the medium surrounding the particle, n_m its refractive index ($n_m = 1.33$ for water), a is the particle radius (1 nm – 10 µm for small micro- and nano- plastics) and λ is the laser wavelength in vacuum (400 – 1100 nm for most standard lasers operating in the NUV – VIS – NIR range). For particles much bigger than the laser wavelength ($x \gg 1$), i.e. for all microplastics, the ray optics approximation is generally used.[84] In the ray optics regime (Figure 2a,b) the optical

field is split in a collection of light rays, each carrying a portion of the total power and linear momentum. When each ray impinges on the particle, it will be partly refracted and partly reflected by the surface, according to Snell's law. Each refracted ray can rebound several times at the surface, travelling inside the particle until it comes out. The total interaction force will be given by the sum of the forces generated by the reflection and refraction of each ray. For a spherical particle the optical force in the ray optic regime can be expressed as:[72]

$$\vec{F} = \sum_k \left[\frac{n_m P_i^{(k)}}{c} \hat{r}_i^{(k)} - \frac{n_m P_r^{(k)}}{c} \hat{r}_{r,0}^{(k)} - \sum_{j=1}^{\infty} \frac{n_p P_{t,j}^{(k)}}{c} \hat{r}_{t,j}^{(k)} \right] \quad (1)$$

where *k* accounts for all the partial incident rays, *j* for all the multiple reflections inside the particles of each transmitted *k*-th ray, $P_i^{(k)}$ is the power of the *k*-th ray incident in the direction $\hat{r}_i^{(k)}$, $P_r^{(k)}$ and $\hat{r}_{r,0}^{(k)}$ are the power and direction of the reflected 0-ray, $P_{t,j}^{(k)}$ and $\hat{r}_{t,j}^{(k)}$ are the power and direction of the transmitted *j*-th ray, *c* is the speed of light in vacuum, n_p is the particle's refractive index.

Preprints (www.preprints.org) | NOT PEER-REVIEWED | Posted: 22 January 2019 doi:10.20944/preprints201901.0227.v1

Peer-reviewed version available at *Environmental Science and Technology* **2019**; doi:10.1021/acs.est.9b03105

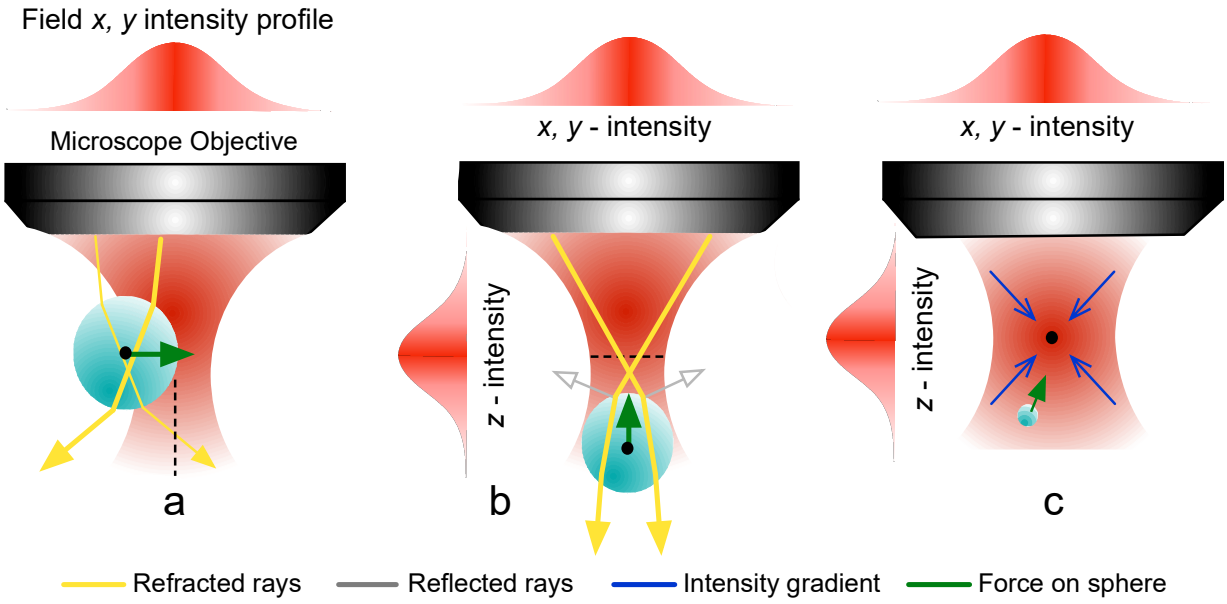

Figure 2. Diagram illustrating the principle of OT. (a) According to the ray optics picture, when a tightly focused beam impinges on a transparent microparticle displaced off the optical axis refraction of rays of different intensity (yellow lines) will impart to the particle a momentum opposite to the one related to the net direction change experienced by the photons. The particle will consequently move under a force (green arrow) proportional to the field intensity gradient, until it reaches the equilibrium position at the optical axis (black dotted line), where the gradient vanishes and the field distribution is symmetric. A similar argument can be applied when the particle is displaced off the center in the axial direction (b). A restoring force pointing towards the intensity maximum (green arrow) arises whenever the transmitted rays (yellow lines) modify the divergence of the beam, exchanging momentum with the particle along the optical axis. This force opposes to the scattering force induced by the reflected rays (gray lines) that, instead, pushes the particle away from the intensity maximum. (c) For small particles (Rayleigh regime) it is the polarisability of the particle that determines the trapping properties. The incident electric field polarizes the particle whose dipole moment will interact with the same field, leading to two forces: a gradient force, that will attract the particle towards the zone of high field gradient (blue lines), and a scattering force pushing it away. In any case, for stable 3D trapping it is necessary (but not sufficient) that the gradient force overcomes the scattering one.

If the particle is displaced laterally with respect to the optical axis (Figure 2a), the component of the net force perpendicular to the incoming ray provides a force proportional to the gradient of the field intensity, the so-called gradient force, that will pull the particle towards the optical axis when $n_m < n_p$ (green arrow in Figure 2a). In Supplementary Figure S1a we plot the transversal component of the gradient force acting on a 10 μm diameter PE bead as a function of the transversal displacement (x) from the spot centre, when the bead is irradiated at 830nm with objectives of increasing numerical aperture ($NA = n_{\mathrm{m}} \sin\theta$, where n_{m} is the refractive index of the medium and θ is objective aperture angle). It is easily noted how, once the sphere enters the laser spot (i.e. $x < 5$ μm) a restoring force attracting the particle towards the equilibrium position ($x = 0$) arises. When the particle is displaced axially below the laser focus (Figure 2b), the overall direction of the laser propagation is not changed, but the divergence is. The transmitted rays (Figure 2b, yellow lines) are refracted in a way that they are more convergent upon leaving the particle. This slight change of the rays' orientation causes a restoring force acting on the particle which is proportional, once again, to the field intensity gradient (longitudinal gradient force) and points upwards. Similarly, if the particle is located above the focus, the transmitted rays become more divergent, leading to a restoring force pointing downwards. The gradient force ($\vec{F}_{\mathrm{grad}}$), whether transverse or longitudinal, causes the trapping of the particle in the laser focus. A second optical force, the scattering force ($\vec{F}_{\mathrm{scat}}$), due to the radiation pressure induced by the recoil of the reflected rays (Figure 2b, grey lines) tends, instead, to destabilize the optical trap by pushing the particle along the beam propagation direction. Stable 3D trapping requires that the gradient force overcomes the scattering force. In the ray optics regime this typically occurs when the numerical aperture of the objective is large enough to create a field gradient capable to counterbalance the effect of the

Preprints (www.preprints.org) | NOT PEER-REVIEWED | Posted: 22 January 2019 doi:10.20944/preprints201901.0227.v1

Peer-reviewed version available at Environmental Science and Technology 2019; doi:10.1021/acs.est.9b03105

radiation pressure. For a 10 µm particle excited at 830nm, the trap loses its stiffness, i.e. its trapping power, when decreasing the NA from 1.3 to 0.6 (Supplementary Figure S1b, magenta, red, blue lines). For NA = 0.3 (green line) the longitudinal force around $z = 0$ is almost flat and the trap becomes unstable. For non-spherical particles, shape dependent optical torques, arising from the exchange of angular momentum between light and particles, can lead to alignment or rotation of the particle.[72] The accuracy of the ray optics approximation increases with the size parameter x, so it is very useful for large particles (e.g. microplastics).

For particles much smaller than the laser wavelength ($x \ll 1$), as for small nanoplastics, we are in the so-called Rayleigh regime in which the dipole approximation can be safely adopted. The advantage of dipole approximation is its simplicity and its ability to make for formal calculations most of the time. The particle is, in fact, modelled as a dipole $\vec{p}$ induced by the incident field $\vec{E}$, i.e. $\vec{p} = \alpha\vec{E}$, where α is the particle's polarizability. For a spherical particle of radius a and dielectric constant ε_p ($\varepsilon_\mathrm{p} = n_\mathrm{p}^2$) immersed in a surrounding medium of dielectric constant ε_m ($\varepsilon_\mathrm{m} = n_\mathrm{m}^2$) we can use the Draine and Goodman expression $\alpha = \alpha_0(1 - i\mathrm{k}_\mathrm{m}^3\alpha_0/6\pi\varepsilon_\mathrm{m})^{-1}$ where k_m is field wave vector, λ the wavelength and α_0 the static polarizability given by the Clausius-Mossotti relation $\alpha_0 = 4\pi a^3\ \varepsilon_\mathrm{m}\left(\varepsilon_\mathrm{p} - \varepsilon_\mathrm{m}\right)/\left(\varepsilon_\mathrm{p} + 2\varepsilon_\mathrm{m}\right)$. The (oscillating) induced dipole will interact electrostatically with the (oscillating) incident electromagnetic field, leading to a force whose time-averaged expression is given by: [72]

$$\langle\vec{F}\rangle = \underbrace{\frac{1}{4}\,\mathrm{Re}(\alpha)\,\vec{\nabla}\left|\vec{E}(\vec{r})\right|^2}_{\text{Intensity gradient}} + \underbrace{\frac{n_\mathrm{m}}{2c}\,\sigma_\mathrm{ext}\,\mathrm{Re}\left(\vec{E}\times\vec{H}^*\right)}_{\text{Radiation pressure}} + \underbrace{\frac{c\,n_\mathrm{m}\,\varepsilon_\mathrm{m}}{4i\omega}\,\sigma_\mathrm{ext}\,\vec{\nabla}\times\vec{\mathrm{E}}\times\vec{\mathrm{E}}^*}_{\text{Polarisation gradient}} \qquad (2)$$

Here $\mathrm{Re}(\alpha)$ is the real part of the particle's polarizability, $\left|\vec{E}(\vec{r})\right|^2$ the intensity profile of electromagnetic field as a function of the position $\vec{r}$, $\vec{H}^*$ is the complex conjugate of the magnetic field, ω the angular frequency, $\sigma_\mathrm{ext} = k\,\mathrm{Im}(\alpha)/\varepsilon_\mathrm{m}$ is the extinction cross section of the particle

in the medium. The first term is the gradient force, proportional to the real part of the polarisability and to the gradient of the field intensity. Particles featuring positive values of $\mathrm{Re}(\alpha)$, such as plastics, will be attracted towards the centre of the optical trap (Figure 2c) and trapped. The second term is the scattering force. It is proportional to the extinction cross section of the particle and to the real part of the Poynting vector of the field. It accounts for the radiation pressure and will tend to push the particle outside the trap. The third term is a spin dependent force. It can arise from polarisation gradients in the electromagnetic field, but usually does not play a role in optical trapping because it is negligible compared to the other contributions when linear polarizations are used. In Supplementary Figures S1(c, d) we show the transverse and longitudinal forces acting on a 90nm PS particle at 830nm excited through objectives of different NA. Again, it is seen that a restoring force attracting the particle in the central position occurs for small displacements from the center, and that objectives with numerical apertures $NA \geq 1$ are necessary to have stable trapping in the longitudinal direction (the longitudinal force is flat for NA =0.6).

In the intermediate regime, typical of large nanoplastics, when the particle size is comparable with the light wavelength ($x \sim 1$) or for highly non-spherical or non-homogeneous particles, a complete wave-optical modelling of the particle-light interaction is needed to calculate the optical forces. Different methods can be considered[66] such as the generalized Lorentz-Mie theory that provides exact results for spherical particles of any size, the Discrete Dipole Approximation in which particles are decomposed in a great number of punctual dipoles, or the T-matrix formalism based on the multipole expansion of the fields which is suitable for dealing with scatterers of (almost) arbitrary morphology.

The limits of validity of the ray optics and dipole approximations have been studied for PS spheres in water at a wavelength of 830nm.[72] Comparing the calculations with the results of a more

accurate T-matrix model, it is found that the dipole model well reproduces the T-matrix results for particles smaller than 100nm, namely for all small nanoplastics, whereas the ray optics regime can be safely applied for particles larger than 1 μm, that is for all microplastics. For large nanoplastics (100nm – 1μm) the approximated models can provide results quite far from the reality. Whatever the model used to calculate the forces, in a stable optical trap and for small displacements from the equilibrium position, the restoring force can be approximated to be proportional to the particle's displacement (Hook's law, Supplementary Figure S1), i.e. $F_l = -k_l \, \Delta r$, where $l = \{x, y, z\}$ indicates the three spatial directions and $k_{x,y,z}$ represent the trap stiffness associated to each coordinate, Δr the particle's displacement along the given coordinate.

Optical trapping of nanoplastics. In order to acquire a Raman spectrum of a micro/nanoplastic particle, measurement times from few seconds up to few minutes are required. Stable optical trapping is therefore needed for Raman tweezers experiments. Predicting under which experimental conditions stable trapping is obtained is important, especially when we shrink the size of the particle and change materials. As seen above, optical forces depend on several experimental parameters. For microparticles, indeed, stable optical trapping is achieved when the refractive index of the particle is larger than that of the medium (water) and when the numerical aperture of the objective is high enough to have a sufficiently steep dependence of the force on the position (Supplementary Figure S1b).

Table 2. Refractive index of common plastic pollutants. The refractive index of polymers is dispersive, i.e. it depends on the light wavelength in a non-linear way.[85] Values measured at the

Preprints (www.preprints.org) | NOT PEER-REVIEWED | Posted: 22 January 2019 doi:10.20944/preprints201901.0227.v1

Peer-reviewed version available at Environmental Science and Technology 2019; doi:10.1021/acs.est.9b03105

sodium *D*-line (589.3nm), n_D, can be found in ref.[86] Extrapolations in the visible – near-infrared can be found in web-databases.[87,88]

Polymer	Refractive index (wavelength)
Polyethylene (PE)	1.51 – 1.54 (589.3nm),[86] 1.49 (833nm)[88]
Polypropylene (PP)	1.49 (589.3nm) [86]
Polystyrene (PS)	1.59 (587.6nm), 1.577 (833nm) [85]
Polyamide (PA, Nylon)	1.53 (589.3nm) [86]
Polyvinyl alcohol (PVA)	1.48 (588nm), 1.47 (828nm) [87]
Polyvinyl chloride (PVC)	1.52 – 1.55 (589.3nm) [86]
Polymethyl methacrylate (PMMA)	1.491 (587.6nm), 1.484 (833nm) [85]
Polyethylene terephthalate (PET)	1.64 (589.3nm) [86]

The refractive index of the polymeric materials varies in the 1.3 – 1.7 range[89] and the values relative to the most common plastic pollutants (Table 2) are indeed larger than that of water (n_w = 1.33). Therefore, using an objective with NA 1.3 (100X, oil immersion), stable trapping is expected in all the size spectrum of microplastics. The same does not necessary hold for nanoplastics, for which the laser power becomes important, in addition to the other parameters. For small enough particles, in fact, the Brownian motion can destabilize the optical trap. Having a gradient force stronger than the radiation pressure is, therefore, a condition no more sufficient to for stable trapping. An additional condition must be fulfilled, i.e the depth of the trapping potential must be deep enough to overcome the kinetic energy of the particle due to the Brownian fluctuations. Simple thermodynamic considerations tell us that this is achieved whenever the Boltzmann factor $R_{\mathrm{therm}} = \exp(-U_{\max}/k_B T) \ll 1$,[69] that is when the thermal energy of the particle ($k_B T$, where T is the absolute temperature and k_B is the Boltzmann constant) is smaller

Preprints (www.preprints.org) | NOT PEER-REVIEWED | Posted: 22 January 2019 doi:10.20944/preprints201901.0227.v1

Peer-reviewed version available at Environmental Science and Technology 2019; doi:10.1021/acs.est.9b03105

than the trapping potential ($U_{\max} = \alpha\,|\mathrm{E}|^2/4$). We can safely assume $U_{\max}/k_{\mathrm{B}}T \geq 3$ to ensure that $R_{\mathrm{therm}} < 0.05$. If we consider a Gaussian beam of power P_0 focused on a diffraction limited waist of size $w_0 = 1.22\,\lambda/NA$, it can be found that stable trapping is expected whenever the laser power exceeds a threshold value given by:

$$P_{\mathrm{thr}} = \frac{1.12\; c\; k_{\mathrm{B}}\; T\; \lambda^2 \left(n_{\mathrm{p}}^2 + 2n_{\mathrm{m}}^2\right)}{a^3 NA^2\; n_{\mathrm{m}} \left(n_{\mathrm{p}}^2 - n_{\mathrm{m}}^2\right)} \qquad (3)$$

The threshold power scales with the square of the wavelength ($P_{\mathrm{thr}} \sim \lambda^2$) and the inverse the particle's volume ($P_{\mathrm{thr}} \sim a^{-3}$), so that higher powers are needed for smaller particles and whenever we use lasers in the NIR. Figure 3a display the trapping threshold power as a function of the radius for a PS sphere. The curves are calculated at the wavelengths of some commonly available lasers (Argon ion, Helium-Neon, Diode, Nd:YAG). Laser beams are assumed to be focused at the diffraction limit with an objective with NA = 1.3. We note that powers of 1 – 10 mW are sufficient to trap particles with diameter ($2a$) in the 200nm range. Conversely, several hundreds of mW are needed to access the sub-50nm regime, which is a more stringent condition. HeNe laser cannot reach such a range, being limited to few tens of mW. Powerful lasers (some Watts) are available at the other wavelengths, indeed. However, power loss due to routing and focusing of the beams, on one side, as well as the occurrence of heating and non-linear effects, on the other, make the sub-50nm range more difficult to access. Figure 3b illustrates the power thresholds needed to trap a 100nm diameter particle made of different materials as a function of their refractive index, at different laser wavelengths. Laser powers of several tens of mW are needed for all the materials, achievable with commercial lasers.

Preprints (www.preprints.org) | NOT PEER-REVIEWED | Posted: 22 January 2019 doi:10.20944/preprints201901.0227.v1

Peer-reviewed version available at Environmental Science and Technology 2019; doi:10.1021/acs.est.9b03105

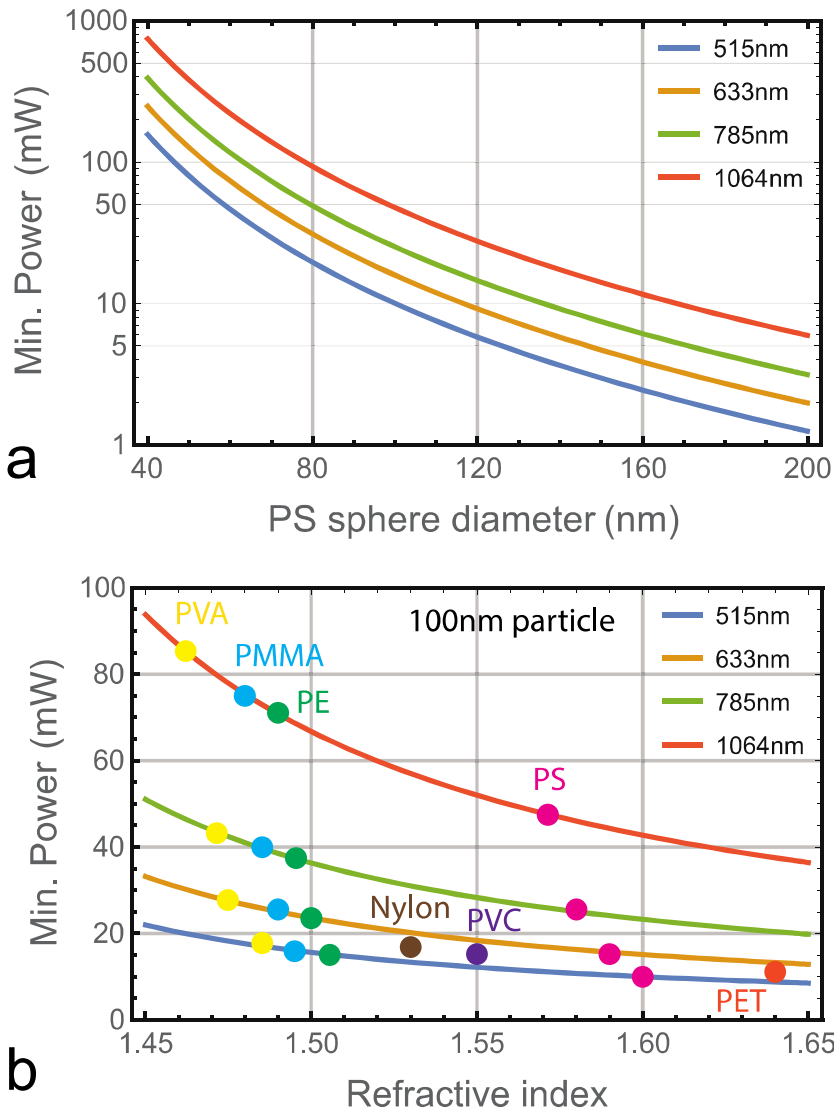

Figure 3: Minimal trapping power for several laser sources (515 nm, 633 nm, 784 nm, 1064 nm) as a function of (a) the sphere diameter ($2a$) for a PS particle at different laser wavelengths, (b) the refractive index (n_p) of a sphere with 100 nm diameter. Values for PVC and Nylon are reported only at 589.3nm, where we have found information on the refractive index.

It is important to note how, in the dipole approximation, the ratio between the gradient and the scattering forces is given by:[69]

$$R_{\text{opt}} = \frac{F_{grad}}{F_{scat}} = \frac{3\sqrt{3}}{16\pi^4} \frac{n_m^3 \lambda^5}{\alpha_0 w_0^2} \quad (4)$$

Preprints (www.preprints.org) | NOT PEER-REVIEWED | Posted: 22 January 2019 doi:10.20944/preprints201901.0227.v1

Peer-reviewed version available at *Environmental Science and Technology* **2019**; doi:10.1021/acs.est.9b03105

For PS particles of diameter smaller than $2a$ = 100 nm we find $R_{\mathrm{opt}} \gg 1$ (at 633 nm in water), so that optical trapping would be always expected, no matter what the laser power is. Accounting for the thermodynamic fluctuations of small nanoplastics is, therefore, necessary if we want to have a realistic prediction of the possibility to trap a specific nanoplastics particle.

EXPERIMENTAL SECTION

Raman Tweezers setup. A RT is basically an inverted microscope that uses a high *NA* objective for trapping, coupled to a Raman spectrometer for signal analysis. The high *NA* ensures, at the same time, the intensity gradient necessary for trapping and the power density needed to maximize the Raman signal. The setup used for our measurements (Figure 4) is a single beam OT. This is, indeed, the simplest experimental configuration possible. Dual-beam setups can be used when high powers are needed for trapping purposes (see Supplementary Figure S2).

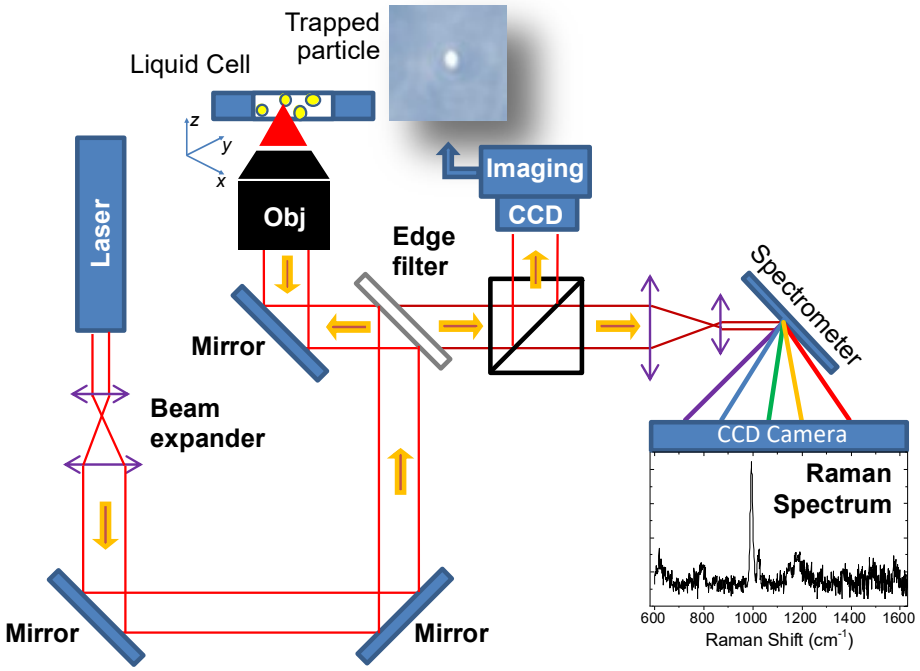

Figure 4. Sketch of the single beam Raman Tweezers setup used in our experiments.

The setup is homemade and takes advantage from the high mechanical stability and versatility offered by optical cage systems (Thorlabs). The apparatus works in a back-scattering configuration, i.e. the Raman emission is collected through the same objective used for excitation and trapping (Olympus 100X, oil immersion, NA 1.3, WD 200 µm). An apochromat water immersion objective (Olympus 60X, NA 1.2, WD 280 µm) can be alternatively used to fully compensate both spherical and chromatic aberrations in the range from the visible to the near-infrared. The RT is coupled to several light sources, namely an Ar^{++} laser (457.9, 476, 488, 515nm, powers P = 10 – 100 mW, Spectra Physics), a DPSS (561nm, P = 50 mW, Oxxius), a He-Ne laser (638nm, P = 25mW, Melles Griot), a diode laser (785nm, P = 50 mW, homemade, laser chip from Thorlabs). The beam is expended with a periscope and sent on two adjustable mirrors for alignment purposes. An edge filter (notch for 785nm) conveys the incident beam to the objective and cuts out most of the Rayleigh scattering (OD = 10^{-7}) from the retro-diffused beam. The laser light is finally focused on glass microchambers containing the particles dispersions. Part of the backscattered beam is sent to a CCD camera (Thorlabs) through a beam splitter to image the sample. Unambiguous size and shape information is retrieved on particles larger than 500nm. Manipulation of the optically trapped particles is achieved by moving the microchamber with the aid of a piezoelectric table (Physics Instrument). A monochromator (Triax 190, Horiba) with 1200 groves/mm gratings is exploited to spectrally disperse the light and a Peltier-cooled (-70°C) silicon CCD camera (1024×256 pixels, Horiba) is used for detection (spectral resolution is about 8 cm^{-1}). For analysis, a drop of solution (10 µL) containing the dispersed particles is cast between a flat microscope slide and a soda-lime coverslip (20x20mm, Forlab) and let it spread in order to cover the coverslip surface entirely, before sealing with nail polish. This enables us to focus on both sides of the cell which is approximately 25 µm thick. In this work, we have used RTs at two

different wavelengths (633 and 785nm) to ascertain which is the best experimental condition in terms of ease of trapping, maximum Raman signal, minimum acquisition time, minimum background (very sensitive to laser wavelength).

Investigated Samples.

PS beads dispersed in distilled water with diameters of 90, 500, 1000 and 2000 nm are purchased from SERVA (90nm) and Polysciences (500, 1000, 2000nm). Nominal particles densities are 3.64 × 10^{11} particles/mL, 4.55 × 10^{10} particles/mL and 5.68 × 10^{9} particles/mL for the 500, 1000, 2000 µm samples. For the 90nm plastics, the producer only provides information on the volume fraction of PS (10%) in the dispersion. Particles were diluted up to 1:10^{7} v/v in in both distilled water and seawater sampled from the Mediterranean Sea, in Torre Faro (Italy). Dilution allowed us to have from some to some tens of particles in the field of view (FOV) of the 100X microscope objective (50×40×25 µm^{3}), and make the process of localization and trapping easy.

PP microparticles were kindly provided by Two H Chem ltd. (Propolder FPP4010). They come in fine particle powder form with a size distribution nominally cantered around 11 µm and standard deviation of 3.5 µm. The powder was first dispersed in distilled water (5 mg in 5 mL). To avoid aggregation, we add 100µL of surfactant (dishwashing liquid) diluted 1:20 v/v in distilled water. For experiments the solution was further diluted 1:100 v/v in distilled or seawater.

Thermoplastic polyamide-6 particles (nylon, melting temperature T_m = 220 °C) were produced by artificial ageing at IFREMER. Polymer sheets 200 µm thick were placed in stainless steel vessels filled with pure water. They were placed in a ventilated oven at 140 °C for 14 days. The internal pressure was set to 15 bars. The resulting solution was used “as prepared” or diluted 1:10 v/v in seawater.

PE particles with diameter between 400 nm and 1.6 µm were prepared at Le Mans University using toluene-in-water emulsions after total dissolution of PE in the toluene phase.[90] Particles feature a concentration smaller than 0.2% (w/w) and are covered with a biosurfactant derived from algae in order to improve stability. The two samples analyzed were prepared dispersed in ultrapure water and in addition of sea salt to reach the typical concentration of seawater (35 g/L).

PVC, PET and PMMA small particles were artificially produced by rubbing against a grinding wet stone for sharpening knives (Norton Abrasives). We started from cm scale plastic fragments extracted from a credit card (PVC), a plastic bottle (PET) and a plastic cup (PMMA). The plastic was rubbed against the stone and then the stone was repeatedly rinsed with the distilled water. The process was repeated three times. No surfactant was added for preliminary measurements in water. Surfactant was added for experiments in seawater (same for PP particles).

Marine sediments were extracted from below the water level of the Torre Faro (Italy) seashore, around the high-tide line, and put in an 8 ml vial with sea water. A drop (20 µL) of surfactant was added and the sample was shaken for 10 minutes to ensure that most sediments get in suspension. Prior to analysis, the sample was decanted for 1 minute in order to let sand and other heavy sediments deposit. Particles in the supernatant were pipetted and directly put in a fluidic cell on our RT setup for analysis.

RESULTS AND DISCUSSION.

Experiments have been carried out with the threefold aim of demonstrating that micro and nanoplastics made of different plastic materials can be easily trapped and quickly analyzed by RT in distilled water (for calibration purposes) and in seawater, that the molecular fingerprints of different plastics present in the same dispersion can be easily discriminated and that the plastics signal can be unambiguously distinguished from the one of mineral sediments present in seawater. A database of the Raman fingerprints of different plastics has been preliminarily acquired for reference purposes, on cm-scale particles in dry conditions, with modes assignment and discussion of the most intense vibrations (Supplementary Figure S3, Supplementary Note 1, Supplementary Tables S1 – S7).

Detection and identification of PS nanobeads. To show that nanoplastics detection is possible down to the small nanoplastics regime (sub-100nm), diluted solutions of PS spheres of 2 µm, 1 µm, 0.5 µm and 90 nm diameter are prepared at concentrations of ~ 10^5 particles/µL, so that some tens of nanospheres are visible under the field of view of our microscope. 10 µL of each solution are pipetted in the microfluidic cell and placed under the RT for analysis at 785 nm (P = 35 mW before the objective). Stable 3D trapping occurs for 1µm and 2µm particles. For 500 nm beads stable 3D trapping is observed only for some seconds, too little for Raman analysis. This is explained with a not perfect overfilling of the objective that lowers the effective NA of the objective and, in turn, worsens the trap stiffness. The measured laser spot is, in fact, ~ 1 µm wide, i.e. slightly larger than the 740nm diffraction limit value. The 90nm particles are always pushed away from the trap, due to the high scattering force component along the optical axis. Stable trapping (2D trapping) can be, however, recovered by pushing the particle against the top part of our sample cell, which will counterbalance the axial pushing force (Supplementary Figure S4). Exploiting the 2D trapping stratagem, we are able to immobilize under the laser spot particles as

small as 90nm. Size determination of the trapped beads is easily achieved down to ~ 500 nm (Figure 5a—d) from calibrated optical images. Below this limit, the size of the particle image will be deeply influenced by diffraction, and will not be representative of the actual particle size. Notably, Raman spectra are easily collected at all sizes, down to 90 nm (Figure 5e). As shown in the inset of Figure 5e (black symbols), the intensity of the 1000 cm^{-1} Raman mode scales as the third power of the particle's diameter (red line), i.e. as the particle's volume for the smallest diameters. Some degree of saturation occurs in the range between 1 and 2 µm diameter. This is expected, since for the 2µm particle the laser spot (diameter $w_r \sim 1\mu m$, depth $w_z \sim 2$ µm) is smaller than the particle and therefore the particle's volume exceeds the Raman scattering volume excited by the laser. Optical trapping and Raman spectroscopy of PS particles (90nm – 2µm) in distilled water has been also obtained at 633nm. In Supplementary Figure S5 we compare the spectra normalized to power and integration time, measured on a 1µm PS bead at 633nm (red line) and 785nm (blue line). The signal at 633nm is ca. 2.5 times more intense, a factor compatible with the λ^{-4} wavelength dependence of the Raman scattering. Further advantages found at 633nm are: a smaller power needed to acquire the spectra (15 mW against 35 mW at 785nm), the reduced measurement time (5s against 10s) and the larger spectral range accessible (200 – 4000 cm^{-1} at 633nm against 200 – 2500 cm^{-1}) due to the limited response of the detector in the NIR. On the other hand, a continuum background is detected at 633nm (black line) when acquiring the spectrum of the liquid, without any particle trapped. This is almost absent at 785nm. The presence of a background signal decreases the signal to noise ratio at 633nm, although not dramatically (19 against 28).

Preprints (www.preprints.org) | NOT PEER-REVIEWED | Posted: 22 January 2019 doi:10.20944/preprints201901.0227.v1

Peer-reviewed version available at Environmental Science and Technology 2019; doi:10.1021/acs.est.9b03105

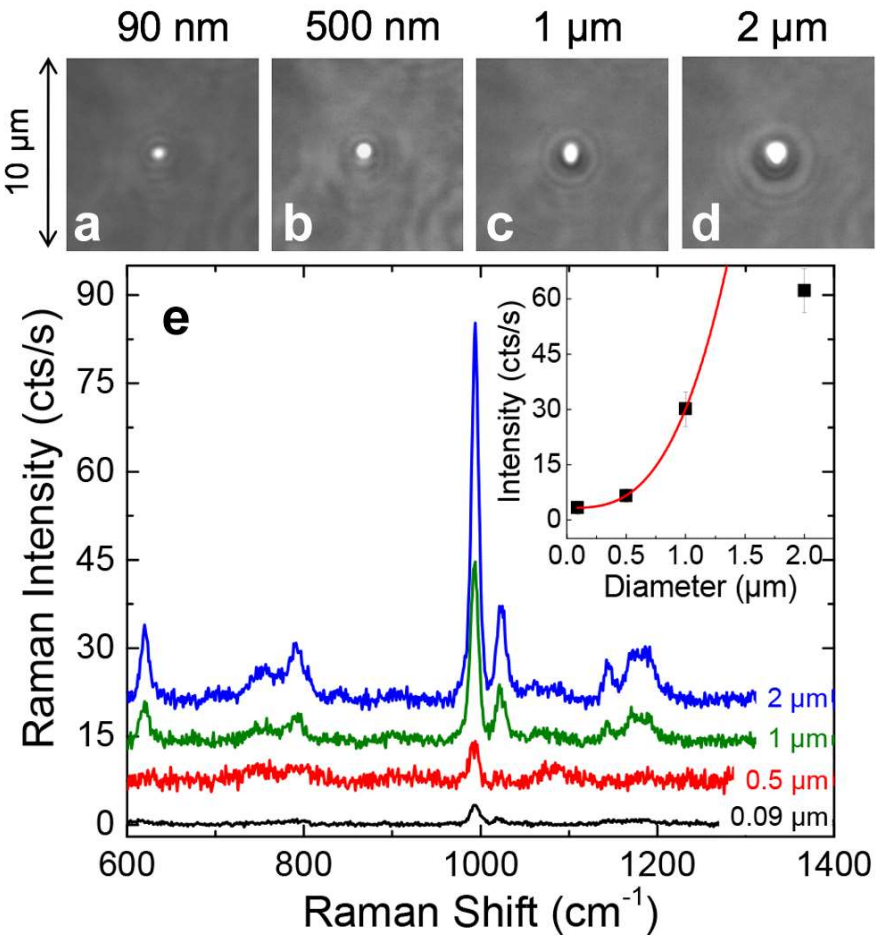

Figure 5: (a – d) Optical images of trapped PS beads from 90 nm to 2 µm diameter in distilled water. (e) Baseline subtracted Raman spectra of optically trapped single PS beads (black to blue lines). Excitation wavelength: 785 nm. Power: 35 mW before the objective. Integration time for *d* = 90nm is 180s (3 acquisitions), for *d* = 500nm is 60s (2 acquisitions), for *d* = 1 and 2 µm is 10s (2 acquisitions). Intensities plotted in (e) are normalized to power and acquisition time in order to be comparable. Spectra are offset for clarity. The inset shows the diameter dependence of the intensity of the 1000 cm^{-1} Raman band (black symbols) and a cubic power fit (red line) reproducing the expected dependence of the signal from the particle's volume for the smallest particles (see text).

Preprints (www.preprints.org) | NOT PEER-REVIEWED | Posted: 22 January 2019 doi:10.20944/preprints201901.0227.v1

Peer-reviewed version available at *Environmental Science and Technology* **2019**; doi:10.1021/acs.est.9b03105

Detection and identification of micro- and nanoplastics in distilled water. Plastic particles of different materials (PET, PA6, PVC, PPMA, PP) have been dispersed in distilled water and analyzed by RT at 633 nm. Optical images of the grinded ones (PET, PA6, PVC, PPMA) show a distribution of sizes from some tens of microns to the sub-micron scale. Different shapes are observed. Commercial PP particles, instead, are quasi-spherical. The observed size distribution is centered around the nominal value of 11 µm. Smaller particles, from 5 µm down to the sub-micron level are also found.

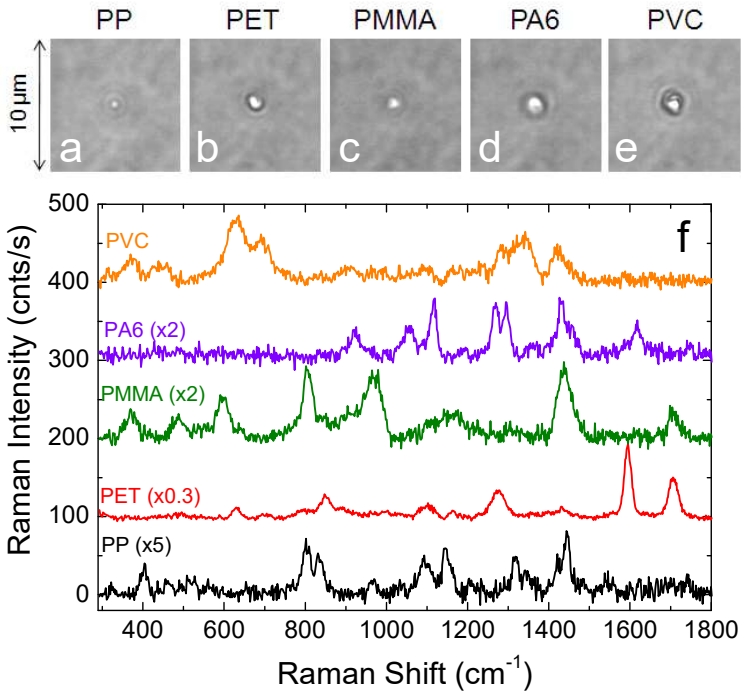

Figure 6: (a – e) Images of micro- (PET, PA6, PVC) and nano- plastics (PMMA, PP) optically trapped in distilled water. Field of view is 10×10 µm^2. (f) Raman spectra of the optically trapped particles, after background subtraction. Excitation wavelength is 633 nm, power is 15 mW before the objective. Integration time for PET is 2s (2 acquisitions), for PMMA is 10s (2 acquisitions), for PA6 is 60s (2 acquisitions), for PVC is 4s (2 acquisitions), for PP is 60s (2 acquisition). Intensities are rescaled in order to be directly comparable (scaling factors indicated in parentheses). Spectra are offset for clarity.

For each material we show in Figure 6 the optical images (a – e) and the Raman spectra (f) of some representative trapped particles, chosen among the smallest found in each sample. The particles diameters span from 2 μm (PVC) to ~ 1μm (PET, PA6), down to the sub-micron scale (PMMA, PP). In all cases, and in particular on artificially aged PA6 small microplastics, we are able to identify the nature of the trapped particles by comparing their Raman spectra to the reference data (Supplementary Figure S3). Small differences in terms of relative intensity of the bands can be attributed to the change in excitation wavelength and the spectral response of the spectrometer.

Detection and identification of micro- and nanoplastics in seawater. RT operation in seawater is somehow complicated by (i) the presence of a more intense background; (ii) the tendency of the smallest particles to form homo- and/or hetero- aggregates; (iii) the presence of microorganisms and mineral particles in the sediments dispersed in seawater. In Figure 7 we show spectra of optically trapped PE particles in seawater, before (a) and after (b) background subtraction, at 633nm (red lines) and 785 nm (blue lines). At 633 nm, the background is 10 times higher that found on distilled water (Supplementary Figure S5), probably due to substances dissolved in the seawater. Nevertheless, the Raman fingerprint of PE is clearly visible in Figure 7(a, red lines), especially when background is subtracted [Figure 7 (b, red line)]. At 785 nm, whenever we focus the laser in proximity of the glass microcell surface, we observe a background signal [Figure 7(a, green line)] consisting of two small peaks just before 1000 cm^{-1} and a broad band cantered ~ 1450 cm^{-1}. This latter originates from the soda-lime coverslip slide fluorescence emission. At 785 nm, as well, PE identification of the optically trapped particle is straightforward and unambiguous [Figure 7 (a, blue line)], especially after background subtraction [Figure 7 (c, blue line)].

Preprints (www.preprints.org) | NOT PEER-REVIEWED | Posted: 22 January 2019 doi:10.20944/preprints201901.0227.v1

Peer-reviewed version available at Environmental Science and Technology 2019; doi:10.1021/acs.est.9b03105

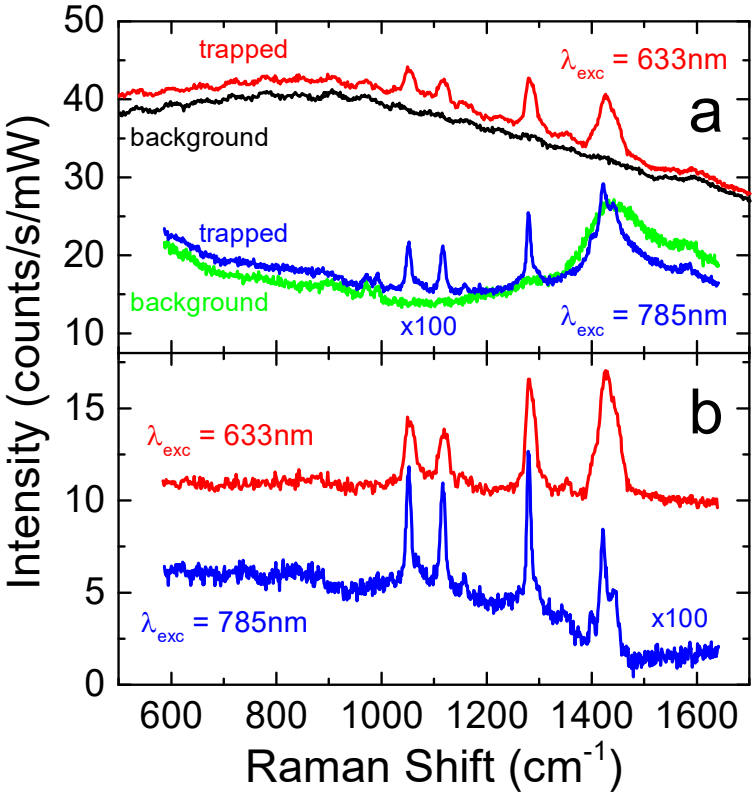

Figure 7: (a) Raman background of seawater (black line) Vs Raman scattering of an optically PE particle dispersed in seawater (red line) measured at 633nm (laser power is 15 mW before objective, integration 20s, 2 acquisitions). Raman background of seawater (green line) Vs Raman scattering of a PE particle trapped in seawater (blue line) measured at 785nm (laser power is 35 mW before objective, integration 300s, 3 acquisitions). (b) Spectra of the PE particles at 633nm (red) and 785nm (blue) after background subtraction. Spectra are normalized to power and integration times, so the signals are directly comparable.

Finally, in Figure 8 we show Raman spectra of optically trapped particles made of different materials, dispersed in seawater. The particles feature dimensions in the micrometer (PET, PVC, PP, PE) and sub-micron (PMMA, PA6) scale and have been chosen among the smallest that can be found in each solution. Measurements carried out at 633nm require integration times ranging from 2s to 60s. Again, unambiguous Raman signatures are found for all the micro and nanoplastics analyzed.

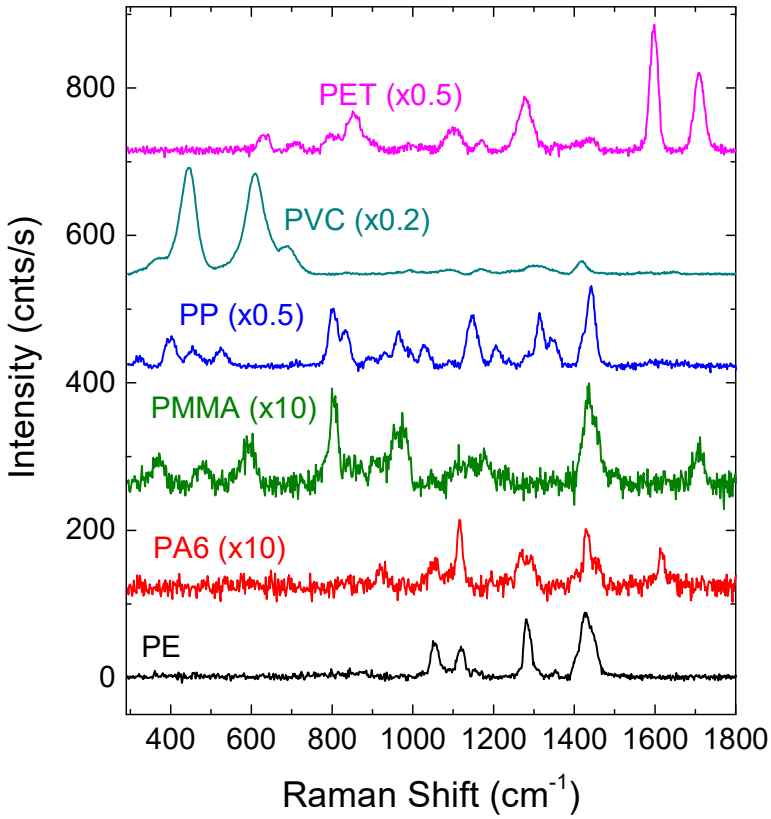

Figure 8: Raman spectra of optically trapped micro- and nano- plastics made of different materials in seawater. Particles dimensions are: PET 2.6 µm, PVC 3 µm, PP 2.8 µm, PMMA sub-micron, PA6: Submicron, PE 2 µm. Laser wavelength 633nm. Power 15 mW, before objective. Integration times are 20 s (2 acquisitions) for PE and PVC, 60s (2 acquisitions) for PA6 and PMMA, 4s (2 acquisitions) for PP, and 2s (2 acquisitions) for PET. Spectra are background-subtracted, rescaled (factors indicated in parentheses) and offset in order to make intensities compared.

Detection and identification of PS sub-100nm nanoplastics in seawater. The use of nanomaterials as a model system to study environmental problems related to microplastics has been recently questioned[15] due to their artificial origin and to the different physical/chemical properties with respect to nanoplastics formed during the natural degradation of microplastic litter (e.g. random shapes, polydisperse dimensions, …). In particular, it is pointed out that nanoplastics

form homo- or hetero- aggregates with other natural or man-produced particles, as it is commonly found in environmental colloidal samples (organic materials, clays). Aimed at demonstrating that individual particles of small nanoplastics (sub-100nm) can be identified by RT also in seawater, we have dispersed therein 90nm diameter commercial PS beads. We observe that PS particles, stable for months in distilled water, aggregate into micron scale structures after few minutes from dispersion in seawater.[91]

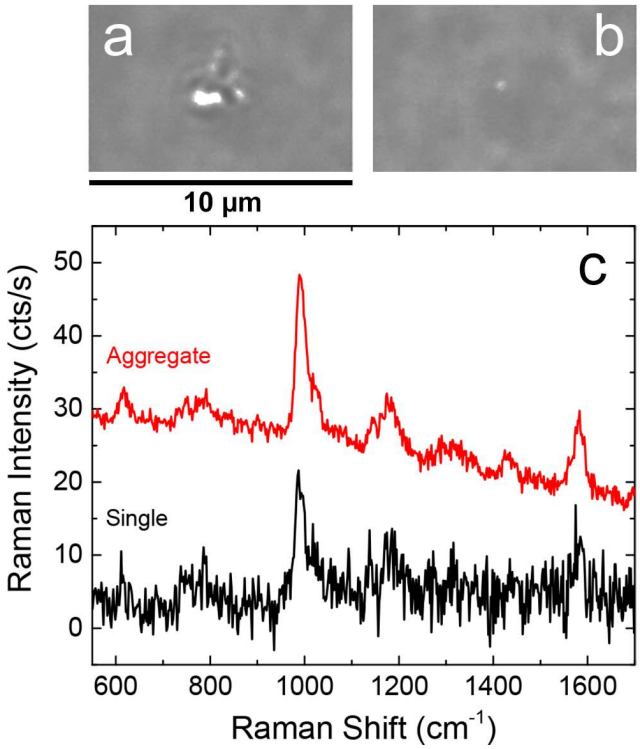

Figure 9: Pictures of a micron scale PS aggregate optically trapped in seawater (a) and of a nanoscale PS particle present in the seawater upon addition of surfactant (b). Raman spectra of the PS particles are plotted in (c). Laser wavelength 633nm, power 15 mW before objective, integration time is 60s (2 acquisitions) for the aggregate and 20s (2 acquisitions) for the single particle. Spectra are normalized to the integration time, so that the intensities are directly comparable.

These aggregates can be easily trapped (Figure 9a) and analyzed (Figure 9c, red line) at 633nm. The PS Raman vibrations are observed superimposed to a background signal. Upon addition of a drop of surfactant and vigorous shaking, however, we have observed nanoscale PS structures, very likely individual 90nm particles. These can be trapped (Figure 9b) and chemically identified (Figure 9c, black line), showing the typical PS Raman fingerprint.

Detection and identification of artificially aged PE particles covered with organic overlayers. Further experiments have been aimed at showing that RT can be used to detect PE microparticles that have undergone ageing in seawater and covered by an organic layer. Two samples of PE are studied, one of them covered with a biosurfactant from microalgae exudates (see Experimental section).[90] At a visual inspection the seawater sample shows precipitated particles, while the other is more "milky", indicating a better dispersion. Raman spectra of optically trapped particles between 0.7 µm and 2 µm display the characteristic bands of PE (Figure 10). The higher intensities generally measured in the seawater sample, are maybe due to the presence of homo-aggregates or particles larger than those present in the sample with the biosurfactant. No Raman fingerprint of this latter molecule is detected, indicating that particles from the natural environment can be identified despite the presence of an eco-corona. In this case, the surface layer is probably too thin to be detected without the help of some signal "enhancement." Finally, we have optically trapped particles in both samples that do not provide any Raman signal (Figure 10, cyan and black lines), although an integration as long as 300s is carried out. These maybe microorganisms or sediments somehow dispersed in the water samples.

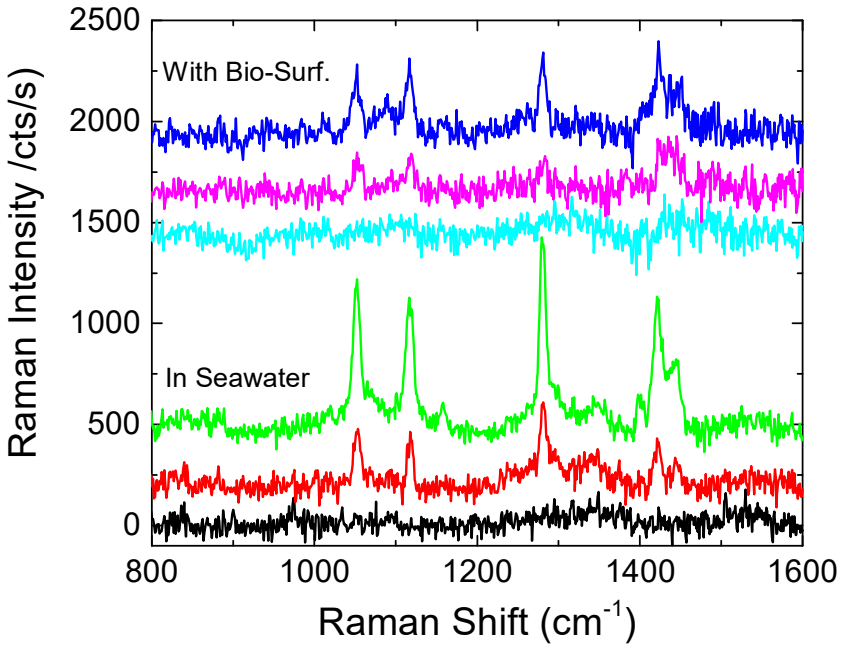

Figure 10. Background-subtracted Raman spectra of PE particles optically trapped in seawater without (red, green) and in presence of the biosurfactant (blue, magenta). Laser wavelength 785nm, power 35mW before objective, integration time 300s, 3 acquisitions. In both samples we found particles that, upon trapping, do not provide any Raman signal (cyan and black lines) even after 15 min integration time.

Detection and identification of micro- and nanostructured sediments in seawater. Marine sediments in form of micro and nanoparticles dispersed in seawater have been optically trapped and analyzed by RT. Spectra are plotted in Figure 11. Modes assignment is reported in Supplementary Note 2. We find particles made of several minerals such as Anatase (pink line), Laumontite (blue line), Calcite (which was the most common, green line), and Alginate (red line). In addition, we find spectra that we attribute to hetero aggregates of Hematite-Jarosite (dark green line) and Hematite-Alginate (black line).

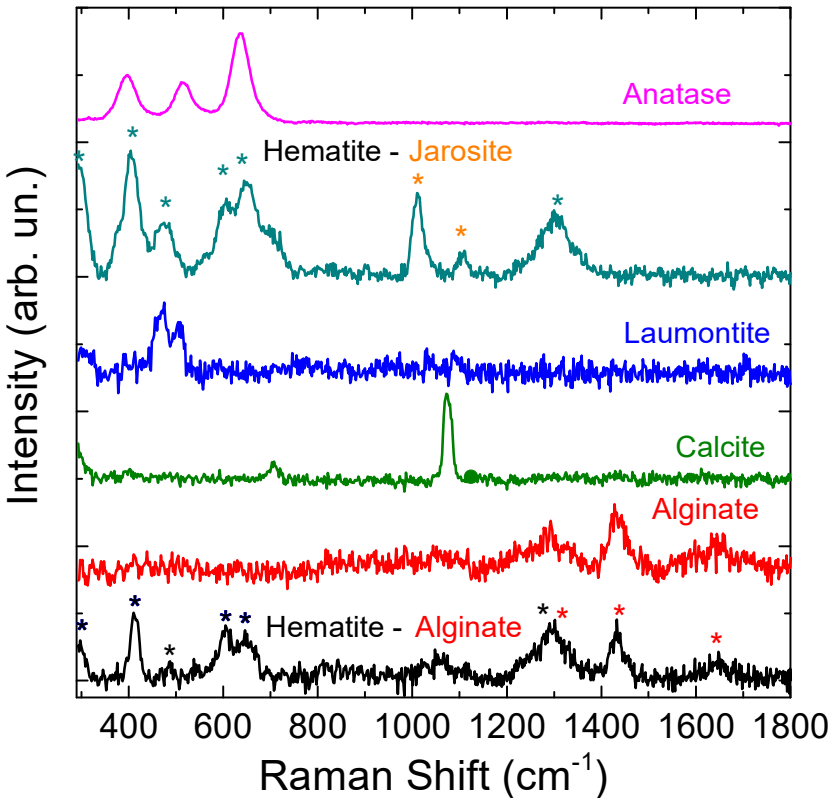

Figure 11. Raman spectra of different sediments dispersed in sea water optically trapped. Asterisks dark green asterisks in the Hematite-Jarosite spectrum (dark green line) indicate the Hematite modes. The orange ones refer to Jarosite. The black asterisks in the Hematite-Alginate spectrum (black line) indicate the hematite modes, the red asterisks the Alginate modes. Excitation wavelength 633, power 15 mW before objective, integration time 20s, 2 acquisitions. Particles dimensions are: anatase 8 μm, hematite-Jarosite 20μm, Laumontite 7 μm, calcite < 1 μm, alginate 1 μm, hematite-alginate 1.4 μm.

Discrimination of different microplastics in seawater. Final experiments have been targeted at demonstrating that we can discriminate different plastics in seawater by using RTs. Experiments have been carried out on seawater dispersions of commercial PP particles. Figure 12 shows an elongated micron scale fiber (a) together with the spheroidal PP particles (b). The Raman

signatures (c, blue and red lines) compared to the reference spectra (green and black lines) allow us to conclude that the spheroidal particle is definitely made of PP, whereas the fiber is composed mostly of nylon. Some weaker peaks (indicated with red asterisks) are compatible with the presence of smaller PP particles, suggesting the occurrence of a hetero-aggregate. The origin of the nylon fiber in the PP microparticles sample is unknown. Some textile fibers could have been accidentally mixed to the PP during fabrication, or maybe the fiber was already present in the seawater sample. This is a very interesting result as micro and nanofibers are suspected to be prevalent in the aquatic environment whereas their detection and identification remains challenging.[92,93]

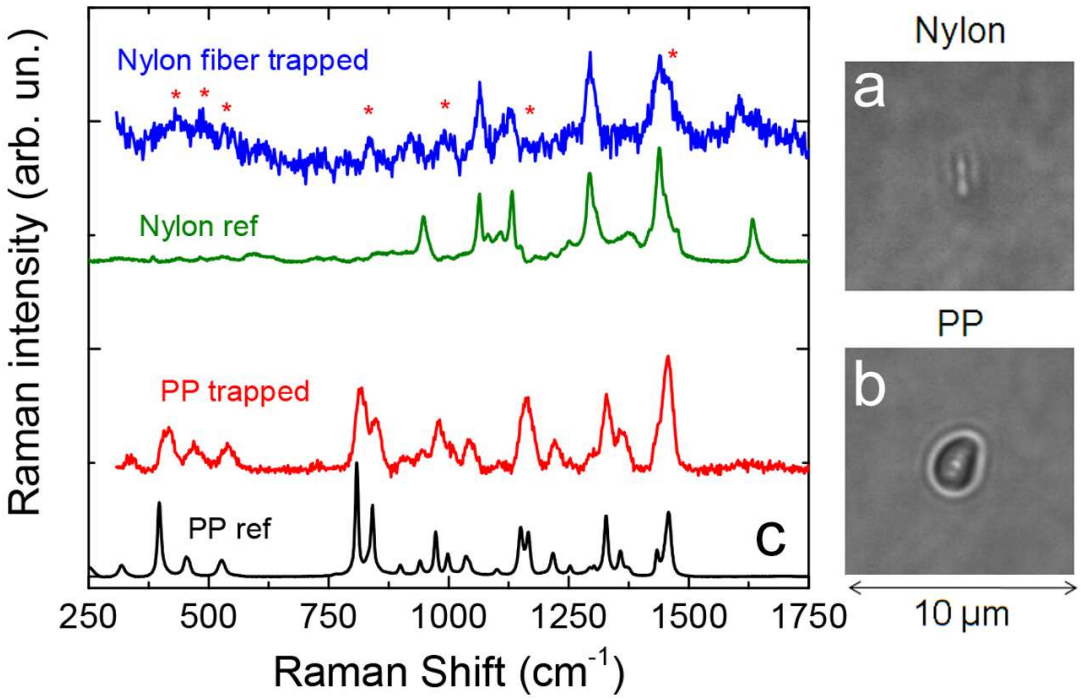

Figure 12. Optical images of a nylon fiber (a) and a spheroidal PP particle (b) dispersed in seawater. (c) Raman spectra of the optically trapped particles (blue and red) compared with the reference spectra (green and black lines) acquired on bulk samples. The red asterisks highlight additional peaks in the nylon spectrum that can be attributed to PP. Excitation wavelength 633nm, power 15 mW before objective, integration times 4s, 2 acquisitions.

Before concluding, we want to stress the fact that all the analysis reported so far is enabled by the capabilities of OT/RT to trap, visualize and analyze a single particle at a time. Experiments carried out on ensembles of particles freely fluctuating, using experimental configurations typical of Raman spectroscopy in liquid (e.g. using a 10X low *NA* objective) do not provide any detectable plastics signal, as shown in the measurements carried out on a PP sample dispersed in seawater (Supplementary Note 3). This is likely due to the fact that the background signal from the liquid overcomes the tiny signal from the sparse plastic particles.

In conclusion, we have shown applications of RTs for chemical analysis in seawater of micro and nanoplastics made of common polymers, with sizes ranging from few tens of microns down to 90nm. RTs enable analysis at the single particle level, overcoming the limitations of conventional Raman spectroscopy in liquid. RTs allow one to optical image and measure the size of the trapped particles down to ~ 500nm, whereas Raman spectra permit unambiguous chemical identification of different plastics in liquid environment. Discrimination of model PP microplastics from small microfibers in seawater dispersions is shown, for the first time. Fast analysis (few seconds per spectrum) is achieved exciting in the visible range (633nm) with powers (15 mW) commonly found in commercial lasers. Signal treatment, namely background subtraction, is however needed, especially in seawater. The use of NIR lasers (785nm) leads to longer analysis times (10 to 100 times), but can be advantageous in terms of a much smaller signal background. The Raman fingerprints of micrometric and sub-micrometric marine sediments have been acquired, and they could be unambiguously distinguished from plastics. Finally, we have shown the capability to quickly identify PE nanoparticles in seawater, despite the presence of an organic layer at their surface. RTs, as all other analytical techniques capable to operate at the single particle level, require concentrated samples. Experiments shown here are easily carried out at ~ 10^5 particles per

mL. This value can be potentially reduced by a factor 100 using wider fields of view (e.g. with 5X or 10X objectives) to spot the particles and then switch to a 100X objective for trapping and analysis. However, a strong effort in terms of particles concentration is needed for real applications in environmental research, as for other analytical techniques such as µRaman, µFTIR, SEM, AFM, etc. RTs, indeed, qualify as a spectroscopic tool useful to study the plastic fate in marine environments and to determine the effect of ageing on plastic particles. Future experimental developments should be directed towards operation in a liquid flow, implementing artificial intelligence routines to spot, count and analyze the particles, and adopt big data analysis tools to treat the thousands of spectra required to provide reliable particles size distributions of different polymeric materials.

ACKNOWLEDGMENTS

N. Micali is acknowledged for fruitful discussions and for providing the PS particles. Two H Chem ltd is acknowledged for providing the PP samples. This work has been funded by IFREMER through the project MERLIN-MICROPLASTIQUE (convention 17/1212947B).

REFERENCES

[1] Thompson, R. C.; Olsen, Y.; Mitchell, R. P.; Davis, A.; Rowland, S. J.; John, A. W. G.; McGonigle, D.; Russell, A. E. Lost at Sea: Where Is All the Plastic? *Science* **2004**, *304* (5672), 838–838. https://doi.org/10.1126/science.1094559.

[2] Law, K. L.; Morét-Ferguson, S.; Maximenko, N. A.; Proskurowski, G.; Peacock, E. E.; Hafner, J.; Reddy, C. M. Plastic Accumulation in the North Atlantic Subtropical Gyre. *Science* **2010**, *329* (5996), 1185–1188. https://doi.org/10.1126/science.1192321

[3] Singh, B.; Sharma, N. Mechanistic Implications of Plastic Degradation. *Polym. Degrad. Stab.* **2008**, *93* (3), 561–584. https://doi.org/10.1016/j.polymdegradstab.2007.11.008.

[4] Carpenter, E. J.; Anderson, S. J.; Harvey, G. R.; Miklas, H. P.; Peck, B. B. Polystyrene Spherules in Coastal Waters. *Science* **1972**, *178* (4062), 749–750. https://doi.org/10.1126/science.178.4062.749

[5] Andrady, A. L. Microplastics in the Marine Environment. *Mar. Pollut. Bull.* **2011**, *62* (8), 1596–1605. https://doi.org/10.1016/j.marpolbul.2011.05.030

[6] Plastic Pellets in the Aquatic Environment: Sources and Recommendations. Final Report. US EPA Oceans and Coastal Protection Division, pp. 117

[7] Zitko, V.; Hanlon, M. Another source of pollution by plastics: Skin cleaners with plastic scrubbers. *Mar. Pollut. Bull.* **1991**, *22* (1), 41-42. https://doi.org/10.1016/0025-326X(91)90444-W

[8] Fendall, L.S.; Sewell M.A. Contributing to marine pollution by washing your face: Microplastics in facial cleansers. *Mar. Pollut. Bull.* **2009**, *58*, 1225-1228. https://doi.org/10.1016/j.marpolbul.2009.04.025

[9] Hernandez, L. M.; Yousefi, N.; Tufenkji, N. Are There Nanoplastics in Your Personal Care Products? *Environ. Sci. Technol. Lett.* **2017**, *4* (7), 280–285. https://doi.org/10.1021/acs.estlett.7b00187.

[10] Stephens, B.; Azimi, P.; El Orch, Z.; Ramos, T. Ultrafine Particle Emissions from Desktop 3D Printers. *Atmos. Environ.* **2013**, *79*, 334–339. https://doi.org/10.1016/j.atmosenv.2013.06.050.

[11] Dubey, M. K.; Bijwe, J.; Ramakumar, S. S. V. Nano-PTFE: New Entrant as a Very Promising EP Additive. *Tribol. Int.* **2015**, *87*, 121–131. https://doi.org/10.1016/j.triboint.2015.01.026.

[12] Gigault, J.; Pedrono, B.; Maxit, B.; Halle, A. T. Marine Plastic Litter: The Unanalyzed Nano-Fraction. *Environ. Sci. Nano* **2016**, *3* (2), 346–350. https://doi.org/10.1039/C6EN00008H

[13] Lambert, S.; Wagner, M. Formation of Microscopic Particles during the Degradation of Different Polymers. *Chemosphere* **2016**, *161*, 510–517. https://doi.org/10.1016/j.chemosphere.2016.07.042

[14] Lambert, S.; Wagner, M. Characterisation of Nanoplastics during the Degradation of Polystyrene. *Chemosphere* **2016**, *145*, 265–268. https://doi.org/10.1016/j.chemosphere.2015.11.078

[15] Gigault, J.; ter Halle, A.; Baudrimont, M.; Pascal, P.-Y.; Gauffre, F.; Phi, T.-L.; El Hadri, H.; Grassl, B.; Reynaud, S. Current Opinion: What Is a Nanoplastic? *Environ. Pollut.* **2018**, *235*, 1030–1034. https://doi.org/10.1016/j.envpol.2018.01.024

[16] da Costa, J. P.; Santos, P. S. M.; Duarte, A. C.; Rocha-Santos, T. (Nano)Plastics in the Environment – Sources, Fates and Effects. *Sci. Total Environ.* **2016**, *566–567*, 15–26. https://doi.org/10.1016/j.scitotenv.2016.05.041

[17] ter Halle, A.; Jeanneau, L.; Martignac, M.; Jardé, E.; Pedrono, B.; Brach, L.; Gigault, J. Nanoplastic in the North Atlantic Subtropical Gyre. *Environ. Sci. Technol.* **2017**, *51* (23), 13689–13697. https://doi.org/10.1021/acs.est.7b03667

[18] Browne, M. A.; Dissanayake, A.; Galloway, T. S.; Lowe, D. M.; Thompson, R. C. Ingested Microscopic Plastic Translocates to the Circulatory System of the Mussel, Mytilus Edulis (L.). *Environ. Sci. Technol.* **2008**, *42* (13), 5026–5031. https://doi.org/10.1021/es800249a.

[19] Cole, M.; Lindeque, P.; Fileman, E.; Halsband, C.; Galloway, T. S. The Impact of Polystyrene Microplastics on Feeding, Function and Fecundity in the Marine Copepod Calanus Helgolandicus. *Environ. Sci. Technol.* **2015**, *49* (2), 1130–1137. https://doi.org/10.1021/es504525u.

[20] Sussarellu, R.; Suquet, M.; Thomas, Y.; Lambert, C.; Fabioux, C.; Pernet, M. E. J.; Goïc, N. L.; Quillien, V.; Mingant, C.; Epelboin, Y.; et al. Oyster Reproduction Is Affected by Exposure to Polystyrene Microplastics. *Proc. Natl. Acad. Sci.* **2016**, *113* (9), 2430–2435. https://doi.org/10.1073/pnas.1519019113.

[21] Tallec, K.; Huvet, A.; Di Poi, C.; González-Fernández, C.; Lambert, C.; Petton, B.; Le Goïc, N.; Berchel, M.; Soudant, P.; Paul-Pont, I. Nanoplastics Impaired Oyster Free Living Stages, Gametes and Embryos. *Environ. Pollut.* **2018**, *242*, 1226–1235. https://doi.org/10.1016/j.envpol.2018.08.020.

[22] Farrell, P.; Nelson, K. Trophic Level Transfer of Microplastic: Mytilus Edulis (L.) to Carcinus Maenas (L.). *Environ. Pollut.* **2013**, *177*, 1–3. https://doi.org/10.1016/j.envpol.2013.01.046.

[23] Setälä, O.; Fleming-Lehtinen, V.; Lehtiniemi, M. Ingestion and Transfer of Microplastics in the Planktonic Food Web. *Environ. Pollut.* **2014**, *185*, 77–83. https://doi.org/10.1016/j.envpol.2013.10.013

[24] Galgani, F.; Hanke, G.; Werner, S.; De Vrees, L. Marine Litter within the European Marine Strategy Framework Directive. *ICES J. Mar. Sci.* **2013**, *70* (6), 1055–1064. https://doi.org/10.1093/icesjms/fst122.

[25] Cózar, A.; Echevarría, F.; González-Gordillo, J. I.; Irigoien, X.; Úbeda, B.; Hernández-León, S.; Palma, Á. T.; Navarro, S.; García-de-Lomas, J.; Ruiz, A. Plastic Debris in the Open Ocean. *Proc. Natl. Acad. Sci.* **2014**, *111* (28), 10239–10244

[26] Imhof, H. K.; Schmid, J.; Niessner, R.; Ivleva, N. P.; Laforsch, C. A Novel, Highly Efficient Method for the Separation and Quantification of Plastic Particles in Sediments of Aquatic Environments. *Limnol. Oceanogr. Methods* **2012**, *10* (7), 524–537. https://doi.org/10.4319/lom.2012.10.524.

[27] Desforges, J.-P. W.; Galbraith, M.; Dangerfield, N.; Ross, P. S. Widespread Distribution of Microplastics in Subsurface Seawater in the NE Pacific Ocean. *Mar. Pollut. Bull.* **2014**, *79* (1), 94–99. https://doi.org/10.1016/j.marpolbul.2013.12.035

[28] Browne, M. A.; Crump, P.; Niven, S. J.; Teuten, E.; Tonkin, A.; Galloway, T.; Thompson, R. Accumulation of Microplastic on Shorelines Woldwide: Sources and Sinks. *Environ. Sci. Technol.* **2011**, *45* (21), 9175–9179. https://doi.org/10.1021/es201811s.

[29] Koelmans, A. A.; Besseling, E.; Shim, W. J. Nanoplastics in the Aquatic Environment. Critical Review. In *Marine Anthropogenic Litter*; Bergmann, M., Gutow, L., Klages, M., Eds.; Springer International Publishing: Cham, 2015; pp 325–340. https://doi.org/10.1007/978-3-319-16510-3_12.

[30] Klaine, S. J.; Koelmans, A. A.; Horne, N.; Carley, S.; Handy, R. D.; Kapustka, L.; Nowack, B.; Kammer, F. von der. Paradigms to Assess the Environmental Impact of Manufactured Nanomaterials. *Integr. Environ. Assess. Manag.* **2012**, 3–14. https://doi.org/10.1002/etc.733@10.1002/(ISSN)1551-3793.InRecognitionofaDistinguishedCareerSteveKlaine

[31] Loos, C.; Syrovets, T.; Musyanovych, A.; Mailänder, V.; Landfester, K.; Nienhaus, G. U.; Simmet, T. Functionalized Polystyrene Nanoparticles as a Platform for Studying Bio–Nano Interactions. *Beilstein J. Nanotechnol.* **2014**, *5* (1), 2403–2412. https://doi.org/10.3762/bjnano.5.250.

[32] Ghislain, L. P.; Switz, N. A.; Webb, W. W. Measurement of Small Forces Using an Optical Trap. *Rev. Sci. Instrum.* **1994**, *65* (9), 2762–2768. https://doi.org/10.1063/1.1144613.

[33] https://www.nist.gov/pml/engineering-physics-division/standard-reference-materials-engineering-physics-division

[34] Török, B.; Kulkarni, A.; DeSousa, R.; Satuluri, K.; Török, M.; Prakash, G. K. S. Synthesis and Application of Polystyrene Nanospheres Supported Platinum Catalysts in Enantioselective Hydrogenations. *Catal. Lett.* **2011**, *141* (10), 1435. https://doi.org/10.1007/s10562-011-0672-5.

[35] Eriksen, M.; Lebreton, L. C. M.; Carson, H. S.; Thiel, M.; Moore, C. J.; Borerro, J. C.; Galgani, F.; Ryan, P. G.; Reisser, J. Plastic Pollution in the World's Oceans: More than 5 Trillion Plastic Pieces Weighing over 250,000 Tons Afloat at Sea. *PLOS ONE* **2014**, *9* (12), e111913. https://doi.org/10.1371/journal.pone.0111913

[36] Sebille, E. van; Wilcox, C.; Lebreton, L.; Maximenko, N.; Hardesty, B. D.; Franeker, J. A. van; Eriksen, M.; Siegel, D.; Galgani, F.; Law, K. L. A Global Inventory of Small Floating Plastic Debris. *Environ. Res. Lett.* **2015**, *10* (12), 124006. https://doi.org/10.1088/1748-9326/10/12/124006

[37] Courtene-Jones, W.; Quinn, B.; Gary, S. F.; Mogg, A. O. M.; Narayanaswamy, B. E. Microplastic Pollution Identified in Deep-Sea Water and Ingested by Benthic Invertebrates in the Rockall Trough, North Atlantic Ocean. *Environ. Pollut.* **2017**, *231*, 271–280. https://doi.org/10.1016/j.envpol.2017.08.026.

[38] Van Cauwenberghe, L.; Vanreusel, A.; Mees, J.; Janssen, C. R. Microplastic Pollution in Deep-Sea Sediments. *Environ. Pollut.* **2013**, *182*, 495–499. https://doi.org/10.1016/j.envpol.2013.08.013.

[39] Suaria, G.; Avio, C. G.; Mineo, A.; Lattin, G. L.; Magaldi, M. G.; Belmonte, G.; Moore, C. J.; Regoli, F.; Aliani, S. The Mediterranean Plastic Soup: Synthetic Polymers in Mediterranean Surface Waters. *Sci. Rep.* **2016**, *6*, 37551

[40] Erni-Cassola, G.; Gibson, M. I.; Thompson, R. C.; Christie-Oleza, J. A. Lost, but Found with Nile Red: A Novel Method for Detecting and Quantifying Small Microplastics (20 µm – 1 mm) in Environmental Samples. *Environ. Sci. Technol.* **2017**, *51* (23), 13641–13648. https://doi.org/10.1021/acs.est.7b04512

[41] Pivokonsky, M.; Cermakova, L.; Novotna, K.; Peer, P.; Cajthaml, T.; Janda, V. Occurrence of Microplastics in Raw and Treated Drinking Water. *Sci. Total Environ.* **2018**, *643*, 1644–1651. https://doi.org/10.1016/j.scitotenv.2018.08.102

[42] Cincinelli, A.; Scopetani, C.; Chelazzi, D.; Lombardini, E.; Martellini, T.; Katsoyiannis, A.; Fossi, M. C.; Corsolini, S. Microplastic in the Surface Waters of the Ross Sea (Antarctica): Occurrence, Distribution and Characterization by FTIR. *Chemosphere* **2017**, *175*, 391–400. https://doi.org/10.1016/j.chemosphere.2017.02.024.

[43] Cole, M.; Lindeque, P.; Fileman, E.; Halsband, C.; Goodhead, R.; Moger, J.; Galloway, T. S. Microplastic Ingestion by Zooplankton. Environ. Sci. Technol. 2013, 47 (12), 6646–6655. https://doi.org/10.1021/es400663f.

[44] Hidalgo-Ruz, V.; Gutow, L.; Thompson, R. C.; Thiel, M. Microplastics in the Marine Environment: A Review of the Methods Used for Identification and Quantification. *Environ. Sci. Technol.* **2012**, *46* (6), 3060–3075. https://doi.org/10.1021/es2031505.

[45] Rocha-Santos, T.; Duarte, A. C. A Critical Overview of the Analytical Approaches to the Occurrence, the Fate and the Behavior of Microplastics in the Environment. *TrAC Trends Anal. Chem.* **2015**, *65*, 47–53. https://doi.org/10.1016/j.trac.2014.10.011.

[46] Renner, G.; Schmidt, T. C.; Schram, J. Analytical Methodologies for Monitoring Micro(Nano)Plastics: Which Are Fit for Purpose? *Curr. Opin. Environ. Sci. Health* **2018**, *1*, 55–61. https://doi.org/10.1016/j.coesh.2017.11.001.

[47] da Costa, J. P. Micro- and Nanoplastics in the Environment: Research and Policymaking. *Curr. Opin. Environ. Sci. Health* **2018**, *1*, 12–16. https://doi.org/10.1016/j.coesh.2017.11.002

[48] Peiponen, K.-E.; Räty, J.; Ishaq, U.; Pélisset, S.; Ali, R. Outlook on Optical Identification of Micro- and Nanoplastics in Aquatic Environments. *Chemosphere* **2019**, *214*, 424–429. https://doi.org/10.1016/j.chemosphere.2018.09.111.

[49] *Raman Spectroscopy for Nanomaterials Characterization*; Kumar, C. S. S. R., Ed.; Springer-Verlag: Berlin Heidelberg, 2012

[50] Dresselhaus, M. S.; Dresselhaus, G.; Jorio, A.; Souza Filho, A. G.; Saito, R. Raman Spectroscopy on Isolated Single Wall Carbon Nanotubes. *Carbon* **2002**, *40* (12), 2043–2061. https://doi.org/10.1016/S0008-6223(02)00066-0

[51] Dorney, J.; Bonnier, F.; Garcia, A.; Casey, A.; Chambers, G.; J. Byrne, H. Identifying and Localizing Intracellular Nanoparticles Using Raman Spectroscopy. *Analyst* **2012**, *137* (5), 1111–1119. https://doi.org/10.1039/C2AN15977E.

[52] Dazzi, A.; Prater, C. B. AFM-IR: Technology and Applications in Nanoscale Infrared Spectroscopy and Chemical Imaging. *Chem. Rev.* **2017**, *117* (7), 5146–5173. https://doi.org/10.1021/acs.chemrev.6b00448

[53] Gucciardi, P. G.; Trusso, S.; Vasi, C.; Patanè, S.; Allegrini, M. Near-Field Raman Spectroscopy and Imaging. In *Applied Scanning Probe Methods V: Scanning Probe Microscopy Techniques*; Bhushan, B., Kawata, S., Fuchs, H., Eds.; NanoScience and Technology; Springer Berlin Heidelberg: Berlin, Heidelberg, 2007; pp 287–329. https://doi.org/10.1007/978-3-540-37316-2_10

[54] Huth, F.; Schnell, M.; Wittborn, J.; Ocelic, N.; Hillenbrand, R. Infrared-Spectroscopic Nanoimaging with a Thermal Source. *Nat. Mater.* **2011**, *10* (5), 352–356. https://doi.org/10.1038/nmat3006.

[55] Felts, J. R.; Kjoller, K.; Lo, M.; Prater, C. B.; King, W. P. Nanometer-Scale Infrared Spectroscopy of Heterogeneous Polymer Nanostructures Fabricated by Tip-Based Nanofabrication. *ACS Nano* **2012**, *6* (9), 8015–8021. https://doi.org/10.1021/nn302620f

[56] Yeo, B.-S.; Amstad, E.; Schmid, T.; Stadler, J.; Zenobi, R. Nanoscale Probing of a Polymer-Blend Thin Film with Tip-Enhanced Raman Spectroscopy. *Small* **2009**, *5* (8), 952–960. https://doi.org/10.1002/smll.200801101

[57] Huth, F.; Govyadinov, A.; Amarie, S.; Nuansing, W.; Keilmann, F.; Hillenbrand, R. Nano-FTIR Absorption Spectroscopy of Molecular Fingerprints at 20 Nm Spatial Resolution. *Nano Lett.* **2012**, *12* (8), 3973–3978. https://doi.org/10.1021/nl301159v

[58] Primpke, S.; Lorenz, C.; Rascher-Friesenhausen, R.; Gerdts, G. An Automated Approach for Microplastics Analysis Using Focal Plane Array (FPA) FTIR Microscopy and Image Analysis. *Anal. Methods* **2017**, *9* (9), 1499–1511. https://doi.org/10.1039/C6AY02476A

[59] Käppler, A.; Fischer, D.; Oberbeckmann, S.; Schernewski, G.; Labrenz, M.; Eichhorn, K.-J.; Voit, B. Analysis of Environmental Microplastics by Vibrational Microspectroscopy: FTIR, Raman or Both? *Anal. Bioanal. Chem.* **2016**, *408* (29), 8377–8391. https://doi.org/10.1007/s00216-016-9956-3

[60] Frère, L.; Paul-Pont, I.; Moreau, J.; Soudant, P.; Lambert, C.; Huvet, A.; Rinnert, E. A Semi-Automated Raman Micro-Spectroscopy Method for Morphological and Chemical

Characterizations of Microplastic Litter. *Mar. Pollut. Bull.* **2016**, *113* (1), 461–468. https://doi.org/10.1016/j.marpolbul.2016.10.051

[61] Araujo, C. F.; Nolasco, M. M.; Ribeiro, A. M. P.; Ribeiro-Claro, P. J. A. Identification of Microplastics Using Raman Spectroscopy: Latest Developments and Future Prospects. *Water Res.* **2018**, *142*, 426–440. https://doi.org/10.1016/j.watres.2018.05.060.

[62] Käppler, A.; Fischer, M.; Scholz-Böttcher, B. M.; Oberbeckmann, S.; Labrenz, M.; Fischer, D.; Eichhorn, K.-J.; Voit, B. Comparison of μ-ATR-FTIR Spectroscopy and Py-GCMS as Identification Tools for Microplastic Particles and Fibers Isolated from River Sediments. *Anal. Bioanal. Chem.* **2018**, *410* (21), 5313–5327. https://doi.org/10.1007/s00216-018-1185-5.

[63] Fries, E.; Dekiff, J. H.; Willmeyer, J.; Nuelle, M.-T.; Ebert, M.; Remy, D. Identification of Polymer Types and Additives in Marine Microplastic Particles Using Pyrolysis-GC/MS and Scanning Electron Microscopy. *Environ. Sci. Process. Impacts* **2013**, *15* (10), 1949–1956. https://doi.org/10.1039/C3EM00214D

[64] Dümichen, E.; Eisentraut, P.; Bannick, C. G.; Barthel, A.-K.; Senz, R.; Braun, U. Fast Identification of Microplastics in Complex Environmental Samples by a Thermal Degradation Method. *Chemosphere* **2017**, *174*, 572–584. https://doi.org/10.1016/j.chemosphere.2017.02.010

[65] Maes, T.; Jessop, R.; Wellner, N.; Haupt, K.; Mayes, A. G. A Rapid-Screening Approach to Detect and Quantify Microplastics Based on Fluorescent Tagging with Nile Red. *Sci. Rep.* **2017**, *7*, 44501. https://doi.org/10.1038/srep44501

[66] Ashkin, A. Acceleration and Trapping of Particles by Radiation Pressure. Phys. Rev. Lett. 1970, 24 (4), 156–159. https://doi.org/10.1103/PhysRevLett.24.156

[67] Jones, P. H.; Maragò, O. M.; Volpe, G. *Optical Tweezers: Principles and Applications*; Cambridge University Press, 2015

[68] Maragò, O. M.; Jones, P. H.; Gucciardi, P. G.; Volpe, G.; Ferrari, A. C. Optical Trapping and Manipulation of Nanostructures. Nat. Nanotechnol. 2013, 8 (11), 807–819. https://doi.org/10.1038/nnano.2013.208

[69] Ashkin, A.; Dziedzic, J. M.; Bjorkholm, J. E.; Chu, S. Observation of a Single-Beam Gradient Force Optical Trap for Dielectric Particles. *Opt. Lett.* **1986**, *11* (5), 288–290. https://doi.org/10.1364/OL.11.000288

[70] Thurn, R.; Kiefer, W. Raman-Microsampling Technique Applying Optical Levitation by Radiation Pressure. *Appl. Spectrosc.* **1984**, *38* (1), 78–83. https://doi.org/10.1366/0003702844554440

[71] Petrov, D. V. Raman Spectroscopy of Optically Trapped Particles. *J. Opt. Pure Appl. Opt.* **2007**, *9* (8), S139. https://doi.org/10.1088/1464-4258/9/8/S06

[72] Polimeno, P.; Magazzù, A.; Iatì, M. A.; Patti, F.; Saija, R.; Esposti Boschi, C. D.; Donato, M. G.; Gucciardi, P. G.; Jones, P. H.; Volpe, G.; et al. Optical Tweezers and Their Applications. *J. Quant. Spectrosc. Radiat. Transf.* **2018**, *218*, 131–150. https://doi.org/10.1016/j.jqsrt.2018.07.013

[73] Xie, C.; Chen, D.; Li, Y. Raman Sorting and Identification of Single Living Micro-Organisms with Optical Tweezers. *Opt. Lett.* **2005**, *30* (14), 1800–1802. https://doi.org/10.1364/OL.30.001800

[74] Casabella, S.; Scully, P.; Goddard, N.; Gardner, P. Automated Analysis of Single Cells Using Laser Tweezers Raman Spectroscopy. *Analyst* **2016**, *141* (2), 689–696. https://doi.org/10.1039/C5AN01851J

[75] Lambert, P. J.; Whitman, A. G.; Dyson, O. F.; Akula, S. M. Raman Spectroscopy: The Gateway into Tomorrow's Virology. *Virol. J.* **2006**, *3* (1), 51. https://doi.org/10.1186/1743-422X-3-51

[76] Wu, M.; Ling, D.; Ling, L.; Li, W.; Li, Y. Stable Optical Trapping and Sensitive Characterization of Nanostructures Using Standing-Wave Raman Tweezers. *Sci. Rep.* **2017**, *7*, 42930. https://doi.org/10.1038/srep42930

[77] Maragó, O. M.; Bonaccorso, F.; Saija, R.; Privitera, G.; Gucciardi, P. G.; Iatì, M. A.; Calogero, G.; Jones, P. H.; Borghese, F.; Denti, P.; et al. Brownian Motion of Graphene. *ACS Nano* **2010**, *4* (12), 7515–7523. https://doi.org/10.1021/nn1018126

[78] Rodgers, T.; Shoji, S.; Sekkat, Z.; Kawata, S. Selective Aggregation of Single-Walled Carbon Nanotubes Using the Large Optical Field Gradient of a Focused Laser Beam. *Phys. Rev. Lett.* **2008**, *101* (12), 127402. https://doi.org/10.1103/PhysRevLett.101.127402

[79] Svedberg, F.; Li, Z.; Xu, H.; Käll, M. Creating Hot Nanoparticle Pairs for Surface-Enhanced Raman Spectroscopy through Optical Manipulation. *Nano Lett.* **2006**, *6* (12), 2639–2641. https://doi.org/10.1021/nl062101m

[80] Patra, P. P.; Chikkaraddy, R.; Tripathi, R. P. N.; Dasgupta, A.; Kumar, G. V. P. Plasmofluidic Single-Molecule Surface-Enhanced Raman Scattering from Dynamic Assembly of Plasmonic Nanoparticles. *Nat. Commun.* **2014**, *5*, 4357. https://doi.org/10.1038/ncomms5357

[81] Fazio, B.; D'Andrea, C.; Foti, A.; Messina, E.; Irrera, A.; Donato, M. G.; Villari, V.; Micali, N.; Maragò, O. M.; Gucciardi, P. G. SERS Detection of Biomolecules at Physiological PH via Aggregation of Gold Nanorods Mediated by Optical Forces and Plasmonic Heating. *Sci. Rep.* **2016**, *6*, 26952. https://doi.org/10.1038/srep26952

[82] Foti, A.; D'Andrea, C.; Villari, V.; Micali, N.; Donato, M. G.; Fazio, B.; Maragò, O. M.; Gillibert, R.; Lamy de la Chapelle, M.; Gucciardi, P. G. Optical Aggregation of Gold Nanoparticles for SERS Detection of Proteins and Toxins in Liquid Environment: Towards Ultrasensitive and Selective Detection. *Materials* **2018**, *11* (3), 440

[83] Ajito, K.; Torimitsu, K. Single Nanoparticle Trapping Using a Raman Tweezers Microscope. *Appl. Spectrosc.* **2002**, *56* (4), 541–544

[84] Ashkin, A. Forces of a Single-Beam Gradient Laser Trap on a Dielectric Sphere in the Ray Optics Regime. *Biophys. J.* **1992**, *61* (2), 569–582. https://doi.org/10.1016/S0006-3495(92)81860-X

[85] Kasarova, S. N.; Sultanova, N. G.; Ivanov, C. D.; Nikolov, I. D. Analysis of the Dispersion of Optical Plastic Materials. *Opt. Mater.* **2007**, *29* (11), 1481–1490. https://doi.org/10.1016/j.optmat.2006.07.010

[86] Billmeyer, F. W. *Textbook of Polymer Science*, Third Edition.; Wiley-Interscience: New York, 1984.

[87] https://refractiveindex.info

[88] https://www.filmetrics.com/refractive-index-database/

[89] https://scientificpolymer.com/technical-library/refractive-index-of-polymers-by-index/

[90] Balakrishnan, G.; Déniel, M.; Nicolai, T.; Chassenieux, C.; Lagarde, F. Towards More Realistic Reference Microplastics and Nanoplastics: Preparation of Polyethylene Micro/Nanoparticles with Biosurfactant. *Environ. Sci. Nano* **2018**. https://doi.org/10.1039/C8EN01005F.

[91] Moncho-Jordá, A.; Martínez-López, F.; Hidalgo-Álvarez, R. The Effect of the Salt Concentration and Counterion Valence on the Aggregation of Latex Particles at the Air/Water Interface. *J. Colloid Interface Sci.* **2002**, *249* (2), 405–411. https://doi.org/10.1006/jcis.2002.8224.

[92] Salvador Cesa, F.; Turra, A.; Baruque-Ramos, J. Synthetic Fibers as Microplastics in the Marine Environment: A Review from Textile Perspective with a Focus on Domestic Washings. *Sci. Total Environ.* **2017**, *598*, 1116–1129. https://doi.org/10.1016/j.scitotenv.2017.04.172.

[93] Mintenig, S. M.; Int-Veen, I.; Löder, M. G. J.; Primpke, S.; Gerdts, G. Identification of Microplastic in Effluents of Waste Water Treatment Plants Using Focal Plane Array-Based Micro-Fourier-Transform Infrared Imaging. *Water Res.* **2017**, *108*, 365–372. https://doi.org/10.1016/j.watres.2016.11.015.